



KfK 3591  
November 1983

# **Simulated Fuel Melt Movement and Relocation in Two Seven-Pin-Bundle Geometries**

**(SIMBATH out-of-pile  
Experiments  $V_{Th}$  74;  $V_{Th}$  79)**

**W. Pepler, P. Menzenhauer, H. Will  
Institut für Reaktorentwicklung  
Projekt Schneller Brüter**

**Kernforschungszentrum Karlsruhe**



KERNFORSCHUNGSZENTRUM KARLSRUHE  
Institut für Reaktorentwicklung  
Projekt Schneller Brüter

KfK 3591

Simulated Fuel Melt Movement and Relocation in Two  
Seven-Pin-Bundle Geometries  
(SIMBATH out-of-pile Experiments  $V_{Th}$  74;  $V_{Th}$  79)

W. Pepler, P. Menzenhauer, H. Will

Als Manuskript vervielfältigt  
Für diesen Bericht behalten wir uns alle Rechte vor

Kernforschungszentrum Karlsruhe GmbH  
ISSN 0303-4003

## Abstract

The SIMBATH program was initiated to investigate the physical phenomena of transient material movement and relocation during transient overpower (TOP) and loss of flow (LOF) driven TOP accidents in LMFBR's. The energy release during the accident is simulated out of pile by the reaction of a thermite mixture. Two 7-pin experiments have been performed using flowing sodium. In both tests the transient material movement has been recorded by X-ray-cinematography at about 1000 frames per second. The tests have been analysed. The dominant physical phenomena governing the material movement have been estimated.

## Zusammenfassung

Simulierte Brennstoffbewegung und Umverteilung in zwei Siebenstabbündeln (SIMBATH out-of-pile Versuche  $V_{Th}$  74;  $V_{Th}$  79)

Das SIMBATH Programm dient der Untersuchung physikalischer Phänomene während transients Materialbewegungen und Umverteilungen. Dabei werden Bedingungen eingestellt wie sie in Schnellen Brutreaktoren unter Leistungs-transienten (TOP) und bei Kühlungsverlust LOF-TOP auftreten könnten. Die Wärmefreisetzung während des Störfalls wird durch eine Thermitreaktion außerhalb des Reaktors simuliert. Zwei Experimente mit 7-Stabbündeln wurden unter fließendem Natrium durchgeführt.

In beiden Versuchen wurde die Materialbewegung durch Röntgenfilme mit etwa 1000 Bilder pro Sekunde festgehalten. Die Versuche sind analysiert und die wichtigsten physikalischen Phänomene, die die Materialbewegung verursachen, festgestellt.

<u>Contents</u>	Page
1. Introduction	1
2. Experimental technique and test set up	1
3. Experimental results	5
3.1 Test $V_{Th74}$	5
3.1.1 Course of main events	5
3.1.2 Characteristic signals measured	6
3.1.3 Dynamic pressure behaviour	8
3.1.4 Dynamic pressures during the initial course of the experiment	9
3.2 Test $V_{Th79}$	10
3.2.1 Course of main events	10
3.2.2 Characteristic signals measured	10
3.2.3 Dynamic pressure behaviour	11
3.2.4 Dynamic pressures during the initial course of the experiment	12
4. Material movement and redistribution	14
4.1 Representation	14
4.2 Overview of material redistribution in test $V_{Th74}$	14
4.3 Detailed interpretation of the material redistribution behaviour for test $V_{Th74}$	15
4.4 Overview of material redistribution in test $V_{Th79}$	18
4.5 Detailed interpretation of the material redistribution behaviour for test $V_{Th79}$	19
4.6 Post test material distribution	21
5. Discussion of some physical details during the course of the experiments	24
5.1 Pin failure behaviour	24
5.2 Influence of gas on the material movement and relocation	25
5.3 Failure mechanism concerning the bundle wrappers	28
6. Summary and Conclusions	29
7. Literature	31
8. Annex: Matrix of the SIMBATH Tests	32

## List of Tables

Tab. I	Overview of Measuring Chains
Tab. II	Test Parameters of the 7-Pin Bundle Experiments $V_{Th}^{74}$ and $V_{Th}^{79}$
Tab. III	Survey of Pressure Events $V_{Th}^{74}$
Tab. IV	Survey of Pressure Events $V_{Th}^{79}$
Tab. V	Test $V_{Th}^{74}$ , Observations from the X-Ray Cine Film
Tab. VI	Test $V_{Th}^{79}$ , Observations from the X-Ray Cine Film
Tab. VII	Considerations concerning the Pin Failure Mechanism
Tab. VIII	Estimated Fraction of Gas in the Measured Void Volume $V_{Th}^{74}$
Tab. IX	Estimated Fraction of Gas in the Measured Void Volume $V_{Th}^{79}$
Tab. X	SIMBATH, Matrix of Performed Tests
Tab. XI	SIMBATH, Testmatrix up to Year 86

## List of Figures

- Fig. 1 Schematic Arrangement of 7-Pin Bundle for Test  $V_{Th} 74$
- Fig. 2 Schematic Arrangement of 7-Pin Bundle for Test  $V_{Th} 79$
- Fig. 3 Schematic Arrangement of the SIMBATH Loop
- Fig. 4 Important Events during Test  $V_{Th} 74$
- Fig. 5 Gas-Sodium-Vapour Volume, Flow, Characteristic Pressure (P2)  $V_{Th} 74$
- Fig. 6 Dynamic Pressure Behaviour of Test  $V_{Th} 74$
- Fig. 7 Details of the Dynamic Pressure Behaviour for Test  $V_{Th} 74$
- Fig. 8 Important Events During Test  $V_{Th} 79$
- Fig. 9 Gas-Sodium-Vapour Volume, Flow, Characteristic Pressure (P1)  $V_{Th} 79$
- Fig. 10 Dynamic Pressure Behaviour of Test  $V_{Th} 79$
- Fig. 11 Details of the Dynamic Pressure Behaviour for Test  $V_{Th} 79$
- Fig. 12 Redistribution of Material and Blockage Build Up  $V_{Th} 74$
- Fig. 13 Course of Temperatures  $V_{Th} 74$
- Fig. 14 Redistribution of Material and Blockage Build Up  $V_{Th} 79$
- Fig. 15 Course of Temperatures and Void Signals  $V_{Th} 79$
- Fig. 16 Post Test Material Distribution in the Test Sections  
 $V_{Th} 74$  and  $V_{Th} 79$
- Fig. 17 Cross Section of the Upper Blockage ( $V_{Th} 74$ ; ML 667)
- Fig. 18 Enlarged Cross Section of the Upper Blockage with spots for  
Local Analysis ( $V_{Th} 74$ ; ML 667)
- Fig. 19 Surface Section of a Layer between Blockage and the Wrapper  
Wall ( $V_{Th} 74$ ; ML 687)
- Fig. 20 Holes in the Wrapper Caused by Melting Attack ( $V_{Th} 79$ )
- Fig. 21 Layer at the Inner Surface of the Second Wrapper ( $V_{Th} 79$ )



## 1. Introduction

As part of the safety analysis of FBR's the failure and meltdown of a single or several fuel elements must be investigated. Such accidents can be initiated by a loss of cooling, e.g. caused by failure of all primary pumps and a simultaneous failure of all shut down systems (LOF), or by an unprotected reactivity insertion (TOP). Earlier experiments [1] with single pins arranged in a cooling channel under stagnant and flowing sodium were primarily aimed at determining the transport behaviour of the hot melt inside the pin towards the location of the pin failure and the material movement in the vicinity of the failure. The seven pin bundle experiments concentrate on the time and spatially dependent movement of the multi component mixtures (thermite as the fuel simulator, cladding, sodium and the simulated fission gas) outside the pins starting from bundle geometry. Additionally the conditions for the build up of blockages in the simulated breeding zones and the related material redistribution are of great interest. The test results are used to verify the newly developed code CALIPSO [2].

## 2. Experimental Technique and Test Set Up

The energy release resulting from TOP or LOF-driven TOP accidents is simulated by the exothermic reaction of an aluminum-ironoxide thermite mixture. The thermite is filled into tubes typically of 7.6 mm diameter over an axial length of 500 mm [3]. The pin construction also simulates the upper and lower breeder zones. The heat release of about 3600 J per centimeter pin length leads to a final maximum thermite temperature of about 3350 K. In order to simulate different burn-up levels the pins can either be pressurized with an inert gas or evacuated. This gas together with gases released during the chemical reaction result in a pressure build up inside the pin prior to failure. Seven pins have been arranged in a hexcan wrapper for the bundle experiments. A schematic diagram of the test set up of two 7-pin bundle experiments is shown in

Fig. 1 and 2. The test section consisted of three parts, the lower dummy zone (simulating the breeder and the lower half of the fuel zone), the thermite zone (fuel zone) and the upper dummy zone (breeding zone). The subchannel data correspond to that of the second core of the FBR SNR 300. The bundle wrapper was surrounded by an annular channel in which sodium flows also but at a lower velocity. For experiment  $V_{Th} 79$  an additional safety channel was mounted around the annular channel to protect the surrounding against leaks (Fig. 2). In case of  $V_{Th} 74$  the upper dummy zone consisted of rather thick walled tubes. For experiment  $V_{Th} 79$  these tubes were altered into pins with smaller wall thickness and a ceramic filling in order to obtain a better thermodynamic simulation of the breeding zone.

The test section are provided with three X-ray sources distributed axially with some overlapping to provide for a continuous monitoring of axial motions. The X-ray picture is transformed and amplified to a visible picture by image amplifiers. High speed cameras running normally with 1000 frames per second recorded the material motion, freezing of molten material and relocation inside the test section during the tests. Furthermore the refilling of the test rig with coolant and residues could be seen. The time resolution is typically 1 ms, where the time for exposure is 0.3 ms per frame. The test sections were mounted in a sodium loop (Fig. 3) with the following main components:

The electromagnetic pump (8-9 bar pressure head in maximum), a control valve V24, two filters to protect the pump and the other parts of the loop against particles, a bypass with the shut off valve V29 and an expansion tank. The inlet and outlet lines of the test section are splitted up into two parts to supply the bundle and the annular channel around it with flowing sodium. The hydraulic conditions like flow resistance and inertia for the outlet lines from the test section up to the expansion tank compare rather well with those in a subassembly upper plenum arrangement. However, the flow resistance and inertia of the inlet section is higher in case of the testsection.

Additionally to the three X-ray cine equipments the test section is instrumented with

- sodium flow meters in the inlet and outlet pipes
- thermocouples
- dynamic pressure transducers
- void detectors
- voltage and ampere meters

The characteristics of the measuring chains are listed in table I.

#### Sodium flow meters in the inlet and outlet pipes

The sodium flow is measured by several permanent magnetic flowmeters. The electric signal is amplified by differential amplifiers and then given to the PCM tape recorder. Before the test the flowmeters are calibrated by a special flowmeter with an accuracy of  $\pm 2\%$ . An estimated temperature drift failure of 1% has to be added to this value.

#### Thermocouples

The sodium temperature is recorded by selected NiCr-Ni thermocouples with 0.5 or 1 mm total diameter. The thermocouple connection at the location of measurement is either of the grounded or isolated type. For well wetted thermocouples of 0.5 mm outer diameter the average response time for the grounded type is ~ 17 ms for the isolated ~ 31 ms. The corresponding value for the 1 mm outer diameter is ~ 62 ms in the average. The standardized measuring error of the thermocouple material is  $\pm 0.75\%$ . To compensate room temperature the thermoelectric voltage is based to a temperature of 50 °C with an error of  $\pm 0.5\%$ .

### Dynamic pressure transducer

The course of the dynamic pressure is measured by axially distributed pressure transducers of the piezoelectric type. The pressure transducers are linked to the test section by sodium filled tubes which are kept at a constant temperature of 250 °C at the location of the transducer. The eigenfrequency of the transducer is 65 kHz. It is connected to a charge amplifier with high input impedance and capacitive counter coupling over a frequency range up to 180 kHz (-3 db). It was found in water tests that a special response characteristic exists for the measuring device consisting of the pressure transducer and the linking tube to the test section. For short pressure peaks less than ~ 2 ms the indicated pressure is twice as high as the real one. This has to be taken into account for the interpretation of the pressure readings.

### Void detector

The void measuring device is based on a three lead thermocouple which allows to measure the temperature and at the same time whether liquid sodium or gas-vapour is present at this location. The void measurement makes use of a carrier frequency amplifier with 10 kHz and a low resistance DC output. The void signal is modified in the amplifier to a voltage signal. Because it is more or less a "yes" or "no" signal a measuring accuracy cannot be attributed. The temperature is treated as described before.

### Current and voltage

The voltage for the ignition of the thermite pins is controlled by variable transformers (2400 kVA / 50 Hz). The time dependent course of the ignition current and the voltage across the pins is measured by shunts of class 0.5. From these values the ignition energy can be evaluated. During the test the ignition current and voltage drop is controlled by a fast acting switch off system. This system is activated as soon as the preselected values are exceeded.

The loop was instrumented, too. However, only those instrumentation will be mentioned, which is relevant for the tests itself.

- flow meters
- static pressure transducers

The flow meters are similar to those of the test section. With the static pressure transducers the absolute pressure in the sodium loop and the pressure drop under static flow conditions is measured. The pressure transducers consist of a NaK filled membrane system and a transducer with electrical output. The reproducibility is  $\pm 0.7\%$  at a maximum tracer temperature of  $700\text{ }^{\circ}\text{C}$ .

The registration frequency for all electrical signals was 20 kHz the transient pressures excepted with 40 kHz. All electrical data are recorded on PCM tape (pulse code modulation). The pictures from the X-ray cine equipment are recorded on 16 mm film material.

### 3. Experimental Results

The main aim of the bundle experiments was to investigate the material relocation and blockage build-up starting from bundle geometry. Important parameters of the tests  $V_{\text{Th}74}$  and  $V_{\text{Th}79}$  are listed in Table II. The most significant difference in the parameter set was the initial gas overpressure inside the pin: 0 bar ( $V_{\text{Th}74}$ ) and 16 bar ( $V_{\text{Th}79}$ ). The pressure build-up due to this gas and to gases released during the chemical reaction was estimated to be 50 bar and 100 bar respectively. The total heat release of the thermite reaction amounted to 1.3 MJ for each bundle.

#### 3.1 Test $V_{\text{Th}74}$

##### 3.1.1 Course of main events

Figure 4 shows seven main phases of test  $V_{\text{Th}74}$ . These phases are related to the time after the first irregularity (time zero) of any ignition current, which was assumed to indicate the onset of ignition. In this schematic representation of the different phases the actual sodium inlet and outlet velocities for the bundle and the annular channel as measured by the flowmeters are marked. At 16 ms after ignition boiling starts locally (phase 1). The boiling region increases until the first pin fails in the lower third of the thermite zone at 117 ms (before phase 2). Because of the preceding boiling

the mixture of molten thermite and gas from the pins is injected into partially voided coolant channels. The liquid sodium is ejected into both up- and down-stream direction with a maximum velocity of 9 m/s. The first visible material movement goes in upward direction as indicated in the figure by an arrow. Some time later the material moves downwards and then upwards again. At phase 3 (243 ms) the pins are totally disintegrated along 2/3 of the thermite loaded zone and the liquid sodium has left the pin bundle. Molten material is moving upwards (downstream) and a first material concentration in the upper thermite and the adjacent dummy zone is observed. The velocity of the multiphase mixture still increases additionally supported by sodium evaporation until at phase 5 (~284 ms), i.e. ~167 ms after the first pin failure, a rather tight blockage has been built up at the lower end of the upper dummy zone and a less tight blockage in the lower dummy zone. The sodium flow at the inlet is zero. At this time the most significant redistribution has taken place. A leak develops through the wrapper into the annular channel. This leads to a pressure relief and an expansion of the multi-phase mixture (phase 5-6). After local sodium vaporization in the outer annular channel even the outer wall fails by melt through (phase 7).

### 3.1.2 Characteristic signals measured

The course of events as characterized in Fig. 4 is illustrated by some measured signals for the first 500 ms in Fig. 5. The phases 1-5 are also indicated on the abscissa. The diagrams are discussed from bottom to top. The pressure P2 measured at the lower end of the thermite zone is characterized by a series of decreasing peaks with a subsequent pressure build up in the channel which lasts over a period of 10-20 ms. The time intervals between the peaks increase with time. The first series of pressure peaks is generated ~17 ms after the first pin failure. The first and the smaller second and third peak series are probably caused by a thermal reaction of the melt with sodium (FCI). As a result of the pressure build up the molten material is dispersed and driven towards the dummy zones of the bundle.

In the two diagrams above signals are shown for the annular channel and the bundle inlet and outlet flow. The outlet flowmeter of the annulus,  $D4_T$ , indicates some oscillations probably induced by the events in the bundle via the upper connection between the bundle and the bypass flow. However, a leakage from the bundle into the annulus can be deduced not earlier than at time 267 ms.

The inlet flow ( $D1_T$ ) into the bundle decreases during the boiling period, the outlet flow ( $D3_T$ ) increases, i.e. a voided zone develops in the bundle. At 17 ms after the first pin failure a sharp flow reversal takes place at the inlet flow meter. The outlet flow increases also rapidly but with some time delay which can be explained by the existence of a twophase region between the location of pin failure and the liquid sodium. The sodium vapour in this region must first be compressed or condensed. After a maximum at ~200 ms the outlet flow velocity decreases until at ~300 ms it is close to zero. This is probably caused by gas bubbles or an axially extended gas void passing through the outlet flow meter  $D3_T$ . At ~284 ms as deduced from the X-ray films a very dense blockage has built up in the upper dummy zone.

In the upper diagram of Fig. 5 the integrated flow signal for the bundle inlet and the difference between inlet and outlet are shown for the bundle and the annular channel. For integration the outlet flow  $D3_T$  has been corrected by taking into account  $D5_T$  for the time beyond 200 ms. The two curves of the differences are therefore a measure for the volume of the void. At the end of the boiling period prior to the first pin failure the void reaches ~25 cm<sup>3</sup> corresponding to 12 cm of bundle length, i.e. the first pin fails into a partly voided zone. After the first FCI the void increases rapidly. It leaves the upper dummy zone 84 ms after the first pin failure - assuming that the void expands over the whole cross section - before the upper blockage is built up. In the annulus an extended voided zone does not develop even after the failure of the wrapper. The inlet flow is never interrupted so that a gas and/or sodium induced void is confined locally. Cooling by the sodium flow in the annulus does not impede the failure of the first wrapper and the subsequent penetration of the hot melt into the annulus. Local heat fluxes into the wrapper must therefore be very high.

### 3.1.3 Dynamic pressure behaviour

The course of the dynamic pressures at different locations is given in Fig. 6 and a survey of pressure events in Table III. In the first line of the table the steady pressures due to friction under the initial sodium flow conditions prior to ignition are listed. To estimate the absolute pressure at a location the static head and the cover gas pressure has to be added to these values. In the adjacent lines the dynamic pressures are listed, i.e. the pressure difference between the mentioned stationary pressures and the actual pressure. The second number behind the dynamic pressure value indicates the duration of the pressure peak at its base.

Three succeeding pressure events are shown in Fig. 6. The general appearance of these events is very much the same. They start with a series of more or less high peaks with small duration between 0.5 and 1 ms ending up in a quasi steady pressure increase. The latter increase is much lower than the peaks itself and declines again within 10-30 ms. The highest pressure peak with 194 bar measured in this test at P1 17 ms after the failure of the first pin must be generated near the lower end of the thermite zone because P2 registered a high peak also. This is not the case for the other pressure transducers. These are apparently decoupled from the location of the actual pressure source by the boiling zone in between. The quasi steady pressure increase at P1 and P2 reaches 16 and 19 bars, which is in accordance with the fact that the higher pressure is measured nearer to the location of the pressure event. At around 22 ms after the high pressure peak at P2 the transducer P3 in the center of the thermite zone, shows a series of pressure peaks without a pressure build up behind. Although with variations the further course of the pressure events show again a combination of high pressure peaks and a succeeding pressure build up. The height the pressure build up differs locally, probably pointing to the actual location of the event. P6 located near the end of the upper simulated breeding zone does not show any reaction, except during the boiling period. This proves that a blockage builds up early between the location P5 and P6, so P6 is decoupled from the events in the test section.



With respect to the origin of the very high pressure peaks it must be anticipated that a local FCI takes place because the pressure peak of 194 bar or even half of this after correction cannot be explained by the gas pressure in the pins.

#### 3.1.4 Dynamic pressures during the initial course of the experiment

The transient pressures during the initial course of the experiment are shown in Fig. 7 . Sodium boiling due to the heat transport from the thermite melt in the pins through the cladding can be identified from the two lower pressure transducer readings up to the time 117 ms. The vapour bubbles probably condense again not far away from their origin. The measured peak pressures which increase with boiling time can either be caused by bubble collapse, a local flash boiling at high sodium superheat or an explosive evaporation at a very local hot spot at the cladding. In earlier tests in water [4] such hot spots have been observed. The highest pressure peaks taking into account the response characteristic of the transducer linked to the test section (see chapter 2) correspond to a sodium saturation temperature close to 1300 °C. The subsequent course of the signals indicates a more steady pressure of 7 bars at P1 and P2 which can be due to released gas from the failed pin. The other pressure transducers show a small increase only. This ends with a sharp pressure peak of 194 bar at P2 indicating the first FCI event. The duration of this peak is less than 0.6 ms, typical of an acoustic behaviour. The other pressure transducers above P1 and P2 are decoupled from the lower part of the thermite zone, where the first pin failed, by the 2-phase region or a blockage at a grid spacer before P3. The energy content of the pressure peaks is very low. The succeeding more steady state pressure build up of about 19 bars over a period of 10-20 ms was estimated to be primarily due to a sodium evaporation induced by the preceding FCI. The behaviour is explained as follows:

During boiling but also after the first pin failure (117 ms) liquid sodium is still fed into the larger part of the thermite zone (see Fig. 5 ), where it gets into contact with molten material. A local FCI is generated at 134 ms. The rather coarsely distributed molten material before the FCI is now dispersed and mixed with the residual liquid sodium. The intensified evaporation of the liquid sodium causes the pressure build up of ~20 bars for 10-20 ms.

### 3.2 Test $V_{Th}79$

#### 3.2.1 Course of main events

In Fig. 8 the main phases of the second 7-pin bundle test  $V_{Th}79$  are presented. In contrast to test  $V_{Th}74$  there is no boiling prior to the first pin failure at 86 ms (phase 1). It must be remembered that the pressure in the pin after the reaction was estimated to be twice as high as in test  $V_{Th}74$ . After pin failure a rapid expulsion of the sodium takes place so that at phase 2 (151 ms) the thermite- and the upper dummy zone is voided completely. A maximum sodium velocity of 20 m/s is measured by  $D3_T$ . At phase 3 (214 ms) all pins have failed and are molten along more than half of the thermite zone. Material movement is upwards. The bundle wrapper has molten through locally in the time interval between phase 2 and 3. This leads to a pressure relief and an ejection of the multiphase mixture from the bundle into the annular channel. At phase 4 (297 ms) all pins are molten along the thermite zone and a rather tight blockage has built up at the entrance to the upper dummy zone. In the following period there is a minor movement of material up and down in the thermite zone. The blockage in the upper part is shorter in axial extent than that in test  $V_{Th}74$ , however it is nearly as tight. The blockage in the lower dummy zone is less dense but has a very high flow resistance.

#### 3.2.2 Characteristic signals measured

Characteristic signals of test  $V_{Th}79$  are presented in Fig. 9 like for test  $V_{Th}74$ . The pressure  $P_1$  near the lower end of the thermite zone shows a series of rather low pressure peaks during the first pin failure at 87 ms. However, the subsequent pressure build up to ~12 bars around 100 ms is rather high causing a rapid expulsion of the liquid sodium from the bundle. The expulsion velocity upwards and downwards is much higher than for  $V_{Th}74$  as can be taken from the diagram. This may be due to the higher gas content in the pins. As a result of the higher velocities the void reaches the upper end of the dummy zone at ~140 ms which is earlier than in  $V_{Th}74$  (at 201 ms). From the course of the flow signal near the annular channel outlet it is deduced that the wrapper wall fails at around 140 ms, thus leading to a pressure relief in the bundle. In contrast to experiment  $V_{Th}74$  the wrapper wall fails very early prior to the complete disintegration of the pins and also prior to the onset of the main

material movement in the bundle. It must therefore be anticipated that a multi-phase jet from a failing pin hits and finally penetrates the wrapper wall. The pin failure behaviour is discussed in chapter 5. At 160 ms the expulsion velocity at the bundle outlet decreases to zero within 120 ms. This is probably due to the fact that a gas-bubble or void has reached the outlet flowmeter  $D3_T$  thus disturbing the signal.

The second series of pressure peaks at P1 (223 ms) is much higher than the first one. However, the subsequent pressure build up in the channel is equivalent to that during the first pin failure. The series of pressure peaks is attributed to a thermal reaction (FCI) between the molten material and sodium in the lower part of the thermite zone. This is supported additionally by the course of the flow signal  $D1_T$  measured at the bundle inlet. The flow signal has recovered some time before the FCI and the integral of the flow signal shows that at the time of the FCI the lower liquid sodium interface has just reached the lower end of the thermite zone. The resulting pressure build up leads to a fast disintegration of the lower part of the thermite filled pins and an intense material movement. Finally at ~240 ms a blockage has build up in the upper dummy zone as observed from the x-ray cine film. The inlet flow of the bundle, which has recovered before, is reversed again at the very moment of the second series of pressure peaks. There is also a blockage built up in the lower dummy zone. It remains porous to some extent. Post test flow measurements at the same pump setting resulted in 14 % of the original flow.

### 3.2.3 Dynamic pressure behaviour

The course of the dynamic pressures at different locations is presented in Fig. 10 together with a survey of the pressure events in Table IV as it was done for test  $V_{Th} 74$ . P3 reproduces the dynamic pressure in the annular channel at the center level of the thermite zone. In general test  $V_{Th} 79$  shows pressure peaks lower than for test  $V_{Th} 74$ , the following pressure build up however is of the same order of magnitude.

The pressure events start at 87 ms with the first pin failure in the lower part of the thermite zone. The first series of pressure peaks is rather low. All four pressure transducers register a pressure event which proves that the first pin fails surrounded by liquid sodium. Neither gas nor sodium vapour is present. The following higher pressure peaks at 215 ms and later were registered by P1 and P2 only. The pressure peaks

are due to a FCI as already explained for test  $V_{Th} 74$ . P4 and P5 are decoupled from the pressure events. During the highest peak with 150 bars at P1 a multi-phase zone between P1, P2 and the other transducers exists and a temporary blockage in the upper parts of the thermite section. This causes the decoupling. Later on, e.g. at 426 ms, the blockage in the beginning of the upper simulated breeding zone explains the decoupling between P4 and P5 and the others. The origin of the pressure events were located by the X-ray cine to be in the lower part of the thermite section.

The velocity of the pressure front (e.g. 42 m/s at 215 ms) moving through the test section could be determined by the time delay of the pressure peaks at P1 and P2 but is also observed from the X-ray cine.

Around 140 ms the wrapper of the bundle fails locally. This event is not very clearly registered by P3. At 426 ms even a small FCI event in the annular channel is registered at P3. This is still more pronounced for the event at 544 ms.

#### 3.2.4 Dynamic pressures during the initial course of the experiment

The first 230 ms of the initial pressure behaviour is shown in Fig. 11 and a survey of pressure events in Table IV. As already mentioned the first pin fails surrounded by liquid sodium. By this event only a mild pressure peak is generated with a maximum of 38 bars at P1 and with a succeeding build up of 12 bars in maximum at P1. This pressure build up is registered by all pressure transducers. The course of the first pressure increase is rather smooth within 1 ms risetime compared to the later observed FCI with 0.3 ms only. Also the succeeding pressure build up is different. There is no decrease after the first series of pressure peaks. From these observations it must be concluded that the course of the initial pressure events is atypical for a FCI but caused by the gas released from the pins.

A higher pressure peak than for test  $V_{Th} 74$  was anticipated for two reasons:

- The initial gas pressure in the pin is twice as high.
- The hot melt is injected into liquid sodium during the first pin failure initiating a FCI.

The latter reason seems not to be the dominant one. It has to be explained why this is not the case: For single pin tests in water it was observed [4] that prior to pin failure a very small hot spot can develop. Later on the pin fails at that location. The first pressure peak may depend on the initial size of the hole before a multi-phase filled void exists around the failure location. So the original size of the failure may be as important as the gas pressure in the pin.

A FCI cannot take place because the high gas content of the injected melt leads to a very fast removal of the liquid sodium from the surrounding of the failure. So an intense mixing of melt with liquid sodium is prohibited.

30 ms after the maximum pressure build up the pressure decreases to ~2.5 bars until the succeeding pressure event takes place now with higher pressure peaks at P1 and P2. The initial high and steep pressure peak at P1 is damped out until it arrives at P2. This indicates that a twophase zone is between P1 and P2 and extends also over the other pressure transducers. It can be deduced from the X-ray film that in the time interval between the first pressure build up and the second pressure series all pins fail in the lower thermite zone. This means successively failing pins do not necessarily generate pressure peaks. Combining the second series of pressure peaks at P1 and P2 with the sodium flow in Fig. 9 it can again be concluded that this series of peaks are due to some kind of FCI in the lower thermite section. The succeeding pressure build up was already explained in connection with  $V_{Th}$  74.

## 4. Material Movement and Redistribution

### 4.1 Representation

The material movement and relocation information obtained from the X-ray cine films of test  $V_{Th}74$  is plotted in Fig. 12 versus the time. The representation is more qualitative and confined to the X-ray viewing areas. Details observed are listed in Table V. In the figure on the left the considered axial levels of the test section are marked for which the average material changes over the cross section were analyzed. The initially thermite loaded zone extends up to a level of 500 mm. A dummy zone is located above this. The arrows indicate the main direction of the material movement. At some arrows the observed material velocities and in a few cases the pressure wave velocities are marked. Before pin failure (prior to 117 ms) the upper and lower limit encloses the initial material distribution inside the bundle. The space between is filled in black. The difference in thickness should not be attributed to a difference in the material concentration. This was nearly constant over the axial length. The difference is arising from deficiencies of cine film analysis. The empty status of the bundle wrapper at a location is given when there are only the two limiting lines left. To improve recognition of the regions where more material is collecting than initially present only the additional material is indicated above the upper line. The different phases shown in Fig. 4 are also marked on the time scale of Fig. 12.

### 4.2 Overview of material redistribution in test $V_{Th} 74$

Before phase 2 at 117 ms the disintegration starts in the thermite zone below 100 mm. For 28 ms the material moves upwards with  $\approx 12$  m/s. However it is visible only in the lower X-ray viewing area. The appearance of the movement is that of a dispersed particle shower. Thus annular flow regimes with low momentum coupling are not yet visible. The pin structure is still visible from time to time during this event. At 145 ms the material movement reverses to downwards. All pins in the lower viewing section are molten at 178 ms. The downward movement of more or less coherent and compacted accumulations of molten materials in a gas or vapour surrounding is rather slow. At 221 ms a pressure front passes from below through the lower viewing areas and disperses the accumulations into clouds of molten particles. By this event the most important up-

wards material movement during this test is initiated. Most of the material is removed from the lower third of the thermite zone and is transported through the upper thermite zone into the upper dummy zone where it freezes and builds up a blockage. The blockage is nearly tight at ~284 ms and furthermore movement of material downstream is interrupted. At phase 5 (168 ms after first pin failure) ~2/3 of the thermite zone is emptied of the initial material. The compacted material in the lower part of the blockage is not frozen at that time so it falls by gravity downwards (upstream direction) through the nearly empty thermite section. Some of this material contacts liquid sodium from below. A small thermal interaction between the molten material and sodium (FCI) initiates a new flow reversal and subsequent material movement downstream. This goes back and forth several times until after about 2 sec all movement is finished and the test section is flooded again with liquid sodium.

#### 4.3 Detailed interpretation of the material redistribution behaviour for test V<sub>Th</sub>/74

In the following a more detailed interpretation of the observed behaviour will be given: The first pin fails (117 ms) rather smoothly by a local melt-through into a partly voided region. The total void at that time corresponds to about 25 cm<sup>3</sup> or an equivalent bundle length

of 12 cm based on the flow cross section of the bundle. The course of the pin disintegration could be as follows: It starts with a very local pin failure (diameter 1-2 mm as observed in [4]) which is increasing by melting off the edge of the hole. At the surface the clad melting temperature is not yet reached except very locally. A lot of gas is released from the local failure or failures with some of the melt. The flow regime inside the pin during the first ms is slug flow (observed in single pin exp. [1]) soon turning to annular mist flow. Because of this most of the molten material is kept in the film at the wall and moves only slowly towards the failure. Otherwise a remarkable material movement should have become evident. The molten material ejected from the pins is finely dispersed by the high gas pressure in the pin. In axial direction above and below the pin failure position the subchannels are still rather cold and liquid sodium is present as film or as compact liquid slugs. The dispersed molten material penetrates into the thermite section (ML 100- 230, Measuring Level) cools down itself but also heats up this section. The material, gas

and vapour movement and expansion is upwards between 117 and 145 ms because during this early time interval the flow resistance in this direction is much smaller than downwards. This corresponds to the hydraulic characteristic of the geometrical undestroyed test set up. At the end of this time interval the void extends up to the ML 300 mm. From the course of some temperatures measured by 0.5 mm TM thermocouples some additional information can be drawn (Fig. 13). Taking into account the average delay time of 3 ms and a time constant of 6 ms, T2 at ML  $\pm$  0 shows at that time a very steep increase in temperature indicating at least sodium boiling temperature in its surrounding whereas T3 located in ML 250 shows a small increase only. At 145 ms the pins in the lower viewing area (ML 99-227) start to disintegrate very fast from below. The material movement is now downwards. The reason for the reversal could well be a temporary blockage build up at the spacer grid close to P3, which can be deduced from the signals of the pressure P1, P2 and P3 in Fig. 6. In addition most of the gas at least from the lower thermite section should be released from the pins, i.e. there is no remarkable overpressure of gas in the pin sections available to finely disperse the molten material and move it upwards. So it moves downwards by gravity.

At 157 ms T2 approaches a maximum and after that decreases again. This agrees well with the course of  $DI_T$  in Fig. 5 which has recovered for a short time. Thus colder sodium penetrates into the lower end of the thermite section. At the same time the temperature at T3 starts to increase very rapidly indicating that the temperature front from inside the pins has reached the subchannels and the pins start to disintegrate also at that location. Shortly after T3 fails suddenly with a FCI event registered by P3 in Fig. 6. The temporary blockage which has probably built up at the spacer grid near T3 is melting off during that time.

Finally at 178 ms all pins in the lower viewing area are molten completely and disintegrated. The molten material however is not in a dispersed state but distributed stochastically in material accumulations still moving downwards.



This ends at 221 ms with a reversal of the material movement which starts through the test section from below. At that time the void has already passed the upper end of the upper dummy zone. Before that time the inlet flow has recovered so that liquid sodium is fed into the section from below. Although not very clearly detectable from the pressure readings there is a pressure increase to  $\approx 6$  bars at P1 and P2 and less at P3 and P4. So a pressure difference is built up along the thermite zone of  $\approx 3$  bars for a time interval of  $\approx 15$  ms. This seems to initiate the material dispersion and main movement upwards. The pressure build up should be caused by a flash evaporation of sodium in the lower entrance section of the thermite zone. This section is already colder than the other ones because several reactions with liquid sodium have taken place before. This explains that the evaporation is not of the type of a FCI. The temperature T4 at ML 500 (Fig. 13) starts to rise immediately after the flow reversal in upward direction. The sodium boiling temperature is reached at 247 ms. T5 starts to rise slowly at that time from the original value.

At 250 ms all pins are completely disintegrated along the thermite zone. Material movement is fully in progress upwards. A new series of FCI's takes place accelerating material movement upwards. At this instance the recovered flow reaches its maximum value. Therefore enough liquid sodium is available to initiate a FCI. Behind the FCI a more steady vapour pressure builds up in the bundle wrapper of  $\sim 20$  bars at P1 which causes a new flow reversal of the inlet flow (D1) in Fig. 5. At 259 ms T4 (Fig. 13) registers a very steep temperature increase caused by molten material arriving from below as can be observed from ML 501 in Fig. 12. 4 ms later the material arrives at ML 600 recognized by the steep increase of T5. It is interesting to note that the steep temperature increase at T4 and T5 starts  $\sim 100$  ms behind the pass of void at the measuring levels. From this behaviour it must be concluded that the build up of

void in the time interval considered is primarily due to the released gas and that the hot molten material penetrates into rather cold structures of the upper dummy zone. 54 ms ( $t = 275$  ms) after the initiation of the main material movement the lower part of the thermite section is nearly empty whereas most of the material has collected in the upper dummy zone. At 284 ms the blockage in the upper part is nearly complete well detected by the readings of the decoupled pressure signal P5 and P6 in Fig. 6. As a consequence of the blockage some dispersed material starts to move downwards again.

At 314 ms compacted material starts to move downwards from the upper dummy zone and falls through the test bundle wrapper as can be taken from Fig. 12. Below the lower viewing area it contacts liquid sodium from the inlet causing at 396 ms a new series of FCI's with pressure build up and a renewed flow reversal of the still molten materials into upward direction. Behind this event a blockage has built up also in the lower dummy zone at the beginning of the thermite zone. This is deduced from the pressure readings at P1 and P2 in Fig. 6. The blockage, however is not so tight as the upper one.

The further course of events has been described already in this section and will not be discussed in detail.

#### 4.4 Overview of material redistribution in test $V_{Th79}$

The differences of the material redistribution of test  $V_{Th74}$  and  $V_{Th79}$  are discussed comparing Figs. 12 and 14 and Table V and Table VI. The upper X-ray viewing area is not shown in Fig. 14, because material movements could not be observed. In test  $V_{Th79}$  the first pin fails at 88 ms ( $V_{Th74}$  at 117 ms) near the lower end of the thermite zone and the first visible material movement starts at 109 ms upwards. The appearance of the first material movement is again that of a particle shower. The pin structure is still visible from time to time until at 190 ms all pins have failed in the lower viewing area. Until ~200 ms the amount of material movement is rather small as can be taken from Fig. 14. In contrast to test  $V_{Th74}$  there is no material movement downwards. At 200 ms the main movement upwards is initiated definitely prior to the passing of a pressure front at 223 ms from below. Behind the pressure

front the material movement is however accelerated very much until at 244 ms a blockage is build up in the upper dummy zone some time earlier than for test  $V_{Th} 74$  ~284 ms. During the time interval between 223 and 244 ms at 233 ms compacted material starts to move downwards however only to be seen in the lower viewing area. Apparently the material from this section moves towards the leak in the wrapper at ML 270 mm and disappears into the annular channel. The material penetrates much less into the upper dummy zone as can be taken from the Figs. 14 and 16. At 394 ms the lower thirds of the pins in the center X-ray viewing area (ML 405-576) are disintegrated, at 525 ms finally the pins are completely disintegrated along the thermite section. This is much delayed compared with 250 ms.

#### 4.5 Detailed interpretation of the material redistribution behaviour for test $V_{Th} 79$

In the following a more detailed interpretation of the observed behaviour will be given:

The first pin fails at 88 ms. As discussed together with the initial course of the pressure at P1 and P2 the rise characteristic seems to be atypical for a local FCI but for a pressure increase by gas release via the leak from the pin. At 95 ms the temperature T1 in ML 150 mm (Fig. 15) starts to rise rapidly indicating the pass of a hot front probably mainly gas and molten thermite mixture. At 109 ms the pin structure is masked by a particle shower moving upwards in the lower X-ray viewing area. It can be taken from figure 14 that a distinct material redistribution is not yet measurable during that time. The expulsion of the liquid sodium from the thermite and the upper dummy zone is much faster than in the case of  $V_{Th} 74$ . In less than 28 ms after pin failure the thermite zone is voided completely ( $V_{Th} 74$ , 46 ms) in 53 ms also the upper dummy zone ( $V_{Th} 74$ , 84 ms). Until time 116 ms, when the upper end of the thermite zone is voided, the clad of the pins is at least partly cooled by the high velocity, cold sodium around. So the outer layers of the clad are still rather cold and capable to withstand some mechanical load. The expansion of the gas takes place through the failures in the lower part of the thermite section. Because annular flow is dominating inside the pin

only a small part of the molten material is released at the failure location although the initial gas pressure in the pin was twice as high as in test V<sub>Th</sub>74.

Some time earlier than 190 ms the leak from the bundle wrapper at ML 170 mm seems to have grown to a size that the multiphase mixture in the lower part of the test section expands mainly into the annular channel. As a result P3 in Fig. 10 increases. The pressure difference across the leak is in the order of 1 bar. For this estimate the static pressures before the transient have been taken into account (see Fig. 11 and Table IV).

At 190 ms all pins have failed in the lower X-ray viewing area. The major quantity of gas seems to be released from the pins. The observation is in accordance with test V<sub>Th</sub>74 that prior to any major material movement and relocation the main portion of the gas is released into the subchannels.

The main material movement starts at 200 ms (Fig. 14). This is 85 ms after the liquid sodium has been ejected from the thermite section. Assuming a starting temperature of 600 °C for the outer layer of the cladding of the pins and the melting temperature (1400 °C) at the inner wall an average heat up rate of ≈8000/s can be estimated. This number implies that there is a high heat transfer which is possible only between the clad and a dense melt under intense contact condition. A similar value was determined in single pin experiments [5]. It can be stated from these observations and considerations that the main material movement does not start prior to a rather complete disintegration of the pins at least over extended axial sections.

The material movement upwards is accelerated by a pressure front from below at 223 ms. This pressure front is initiated by some kind of a FCI as already discussed in connection with the pressure signals. At the same time T5, ML 450 mm in Fig. 15 indicates a rapid temperature increase and the subsequent failure of thermocouple. Again the sodium vapour seems to have triggered the main material movement. At 233 ms the material movement in the lower X-ray viewing area is now downwards in the center area still upwards. The higher pressure build up at P1 and P2 has decreased which is mainly due to the fast expansion

through the leak in the wrapper into the annular channel. This can also be seen from the growth of the void in the annular channel in Fig. 9.

Finally at 244 ms a dense blockage is built up at the entrance of the upper dummy zone. It is interesting to note that the pin structure in the center X-ray viewing area still exists in contrast to  $V_{Th} 74$ . I.e. the material is transported through subchannels towards the upper dummy zone where it freezes. The material is colder than in case of  $V_{Th} 74$  because it has to pass through the upper bundle structure which must be at least below the melting temperature of the outer layers of the pin clad. At 394 ms the lower third of the pins in the center X-ray viewing area are disintegrated and finally at 525 ms the active length is broken up.

The different behaviour of the material movement, bundle melting and material relocation must be attributed to the higher gas pressure in the pins. The pins fail earlier in test  $V_{Th} 79$ . Concerning the pin failure behaviour it is referred to chapter 5. There is also a very early failure of the wrapper leading to a fast expansion of the multi-phase mixture into the cold annular channel. Post test analysis showed a lot of additional holes in the wrapper through which the hot melt could escape into the cold annular channel. By this a lot of energy is withdrawn rather early from the system so the stubs of the pins needed a longer time to melt down completely.

#### 4.6 Post test material distribution

The quantitative post test material distributions in the two test sections are shown in Fig. 16 together with the initial distributions. The values are gained by cutting the test sections (first hexcan included only) and weighing the pieces of different length. The related length is indicated in the Fig. 16. In both tests between 65 and 70 % of the initial material has disappeared from the thermite zone. In case of test  $V_{Th} 74$  a more compact

blockage of  $\approx 100$  mm axial extent has been built up in the upper dummy zone compared to the less dense blockage in test V<sub>Th</sub>79. In the first case the blockage starts 100 mm above the thermite zone whereas in the second case the blockage is located at the upper end of the thermite zone. From the overall material balance over the test section it was found that in test V<sub>Th</sub>74 21 % of the material has disappeared in test V<sub>Th</sub>79 27 %. In case of test V<sub>Th</sub>74 this material was probably distributed into the surrounding through the leak in the outer hexcan. In test V<sub>Th</sub>79 the material was mainly carried into the sodium loop via the outer annulus surrounding the bundle wrapper.

The local material distribution and concentration of test V<sub>Th</sub>74 was analyzed for some local spots with an electron beam X-ray absorption method. Fig. 17 shows the cross section of the upper blockage in ML 667. In Fig. 18 which is an enlarged section the analyzed spots are marked. There is a tendency of a separation of the material from the clad, ignition tube, the iron from the thermite mixture and the aluminum oxide. The main corpus of the blockage, spots 2 and 3, consists of the first materials with nearly pure enclosures of aluminum oxide (spot 4). Most of the molten material in the blocked dummy section stayed in a liquid status for some time, so that the oxide and the metal phases could separate.

The surface section of a layer between the blockage and the wrapper wall is shown in Fig. 19. This layer remained after removing the wrapper wall from the blockage. The general impression by microscopic analysis is that the wrapper wall has never molten in this region. So it can be assumed that the layer was built up very early during the test and not restructured afterwards. As long as a surface area of  $3.6 \times 2.8$  mm is averaged it has a similar composition as explained before. When the analysed surface is getting smaller (area of analysis  $450 \times 380$   $\mu\text{m}$ ) enclosures can be found where the metallic components dominate and the  $\text{Al}_2\text{O}_3$  is missed nearly completely.

At the inner surface of the wrapper wall, opposite to the surface described before, more  $\text{Al}_2\text{O}_3$  is found on the average (area of analysis  $8 \times 6$  mm). The other constituents seem to correspond to be structural material of the wrapper.

Test V<sub>Th</sub>79 was analysed similarly as V<sub>Th</sub>74. In the thermite section there are a total of 7 holes from melting attack to the bundle wrapper wall. Some of these can be seen in Fig. 20. The holes vary between 8 - 35 mm, the larger ones elongated into axial direction by a factor of  $\approx$  two. At the outer surface of the bundle wrapper and the inner surface of the second wrapper for the annular channel material is frozen in porous, irregular layers of 0.2 - 1.0 mm thickness with metal slugs and droplets embedded (Fig. 21).

The analysis of the surface of the layer at the inner wall of the bundle wrapper seems to be a mixture of thermite and the clad material. At the outside of this wrapper - the layers are also thinner there - more Al<sub>2</sub>O<sub>3</sub> is found. This can be correlated with the observation (see section 4) that the bundle wrapper in the lower part failed rather early during this experiment. Most of the clad material is not yet molten. So the hot material injected into the annular channel should be very hot thermite primarily. This determines the layer in the annular channel. In the bundle wrapper the clad of the pins melts at a later time and then the main material movement takes place upwards. This could have modified the initial thin thermite layer so that now clad material is included. This should be considered as a hypothesis which is not proven.

## 5. Discussion of some Physical Details during the Course of the Experiments

### 5.1 Pin failure behavior

The initial test conditions for the two cases considered were the same except the pressure in the pins prior to the test. Therefore the feedback of this test parameter on the course of the experiments in the initial phase is roughly estimated.

The burst pressure stress values are applied on the pin cladding for different temperatures. The estimated necessary minimum clad thickness values are listed in Table VII together with the additional assumptions. The actual clad thickness in the two tests is 0.3 mm. As long as the estimated thickness is below the actual one the pin should not fail during the short period of time available, if it is much above, it should fail instantaneously.

The calculated cases in the table correspond to test V<sub>Th</sub>74 and V<sub>Th</sub>79. In case V<sub>Th</sub>74 the pin must not fail by the inner overpressure even when the boiling temperature is reached at the outside. There is still a margin between the estimated necessary clad thickness of 0.2 mm and the actual one with 0.3 mm. A part of the wall can even melt prior to the initial failure.

This is different for case V<sub>Th</sub>79. The necessary wall thickness estimated is higher than the actual one. So the pin must fail prior to reaching the boiling temperature outside. The estimated failure characteristic agrees with the observations from the two tests, although quasi stationary conditions were assumed for the calculation.

Differences in the initial course of the two experiments can be explained by the failure characteristics.

In test V<sub>Th</sub>74 boiling prior to pin failure is possible and was observed (see Fig. 5). The pins fail as soon as a part of the wall is molten. At that time the average wall temperature is higher than in test V<sub>Th</sub>79. Here the pin should fail at an average temperature between 900 - 1000 °C.



So the starting conditions for the further pin disintegration are different for the two tests:

- $V_{Th}$  74 clad is partly molten from the inside, the outside is at boiling temperature or even higher
- $V_{Th}$  79 the clad is not molten except very locally, the outside is  $100 - 150^{\circ}$  below boiling temperature

After pin failure the ejected hot mixture heats up the clad from outside in addition to the melting from inside. The gas from the pins is released very fast because of the dominating annular flow regime. So the overall melting temperature for the clad wall is reached for test  $V_{Th}$  74 after a short period of time. The pins start to disintegrate over the whole length. In case of test  $V_{Th}$  79 the gas and the hot melt is injected into rather cold subchannels and then the hot material starts to heat up the colder clad from outside. Again the gas from the pins is released very fast carrying probably some more molten material with it than in the test before. Because of the lower average clad temperature the clad strength is still high after the main gas pressure relief so that the further pin disintegration needs two times longer compared with  $V_{Th}$  74. This effect is strengthened by the early failure of the bundle wrapper, so that a part of the hot material from the pins does not pass the subchannels but is directly disappearing into the cold annulus.

## 5.2 Influence of gas on the material movement and relocation

The release of the gas from the pin can be roughly estimated taking into account the following information:

- The known initial gas content after the reaction
- X-ray cine film, which show where the pins fail and are disintegrating
- the determined void in the test section
- thermocouple readings at different locations in the thermite zone
- pressure measurements at different locations

For the two tests the results of this estimate is given in Table VIII and IX. In the last two columns the total void and the ratio of the void due to gas only to the total void is listed. It can vary between 0 and 100 %. The latter means that the void exists from gas only.

In case  $V_{Th}^{74}$  prior to any pin failure the void must consist of sodium vapour only. 16 ms later at 133 ms already 30 % of the gas inventory seem to be released into the subchannels. The portion of gas in the void is now 40 %. If 30 % of gas is released from the pins within 16 ms an average gas velocity of 48 m/s must exist in the outlet pin cross section (based on the inner diameter of the pin) at the pin failure. For this estimate annular flow for the thermite and the gas at a subchannel pressure of 8.7 bars is assumed. The high gas velocity at the outlet reduces very fast inside the pin, e.g. to 6 m/s in the axial center of the thermite region. In the further course of the experiment a gas velocity with respect to the pin cross section can no longer be defined because whole pin sections disintegrate. At 174 ms the portion has increased to 55 %. Up to that time a real quantitative material movement cannot be measured although an upward material movement is observed in the X-ray films. Around 147 ms the pressure in the failed pin region (P1, P2) is near 20 bars during a time interval of 10-20 ms, so that a further gas and material release should be interrupted. This pressure is close to the residual pressure in the pins when 40 % of gas are released. The pressure falls again so that at 232 ms 70 % of gas is released and the highest gas portion of 90 % is reached. The main material movement upwards is initiated at 232 ms when a fast sodium evaporation in the lower thermite section takes place (see section 43). So it must be concluded that the sodium evaporation is at least as important for the material movement in the subchannels as the gas released from the pins. At 265 ms gas is released from the pins, its influence vanishes until finally the sodium vapour is the only agent driving the material upwards.

In test  $V_{Th}^{79}$  the pins fail prior to any boiling in the subchannels. Because of the higher gas inventory in the pins the average gas velocity estimated for the outlet pin cross section during the time interval between 88 ms and 101 ms is nearly twice as high with 86 m/s. 12 bars are assumed

as the subchannel pressure at the location of the failed pin cross section. At 101 ms the void exists to 63 % (Table IX) from gas. The influence of gas increases up to ~ 100 % at 201 ms. At that time all pins have failed the main material movement however has not yet started. This compares well with the test  $V_{Th}74$  described before. Finally the main material movement is initiated at 228 ms behind a pressure front due to a fast sodium evaporation at the lower end of the thermite section. This pressure front moves through the test section from below (see Fig. 24). Again the sodium evaporation seems to have triggered the main material movement.

### 5.3 Failure mechanism concerning the bundle wrappers

It is shown in chapter 3 that leaks increasing with time developed from the first wrapper into the annular channel for test V<sub>Th</sub>74 starting at  $\approx 167$  ms after first pin failure and for test V<sub>Th</sub>79 much earlier at  $\approx 56$  ms.

The appearance of the failure indicate a local attack of the wrapper wall which increases more or less by melting off the corners of the original leak hole. There are other locations at the inner wall of the first wrapper with local attacks however penetrating the wall not completely.

The wall of the second wrapper opposite to the failure of the first wrapper i.e. across the annulus is also havily attacked apparently by impinging of a hot multiphase jet from the failure of the first wrapper. At some locations this second wrapper is also molten through after some time delay of several 100 ms. In the following the conditions for the initiating failure mechanism of the first wrapper wall will be evaluated roughly. Because of the rather low sodium velocity; in the annulus the critical heat flux values for saturated pool boiling are applied. The experimental data gained by Noyes [6] for critical heat flux conditions range from 400 to 500 W/cm<sup>2</sup> for the sodium pressure at the location of the failure. In the wrapper with a 2 mm wall a temperature difference of  $\Delta T = \approx 416$  K would exist for such a heat flux. The thermite melt however is even above 3000<sup>o</sup>C so the critical local heat flux conditions are reached easily. In the case considered subcooled boiling conditions may exist. Although not available in the literature the critical heat flux values must be assumed 2 - 4 times higher than for saturated pool boiling, e.g. 2000 W/cm<sup>2</sup>. The necessary maximum  $\Delta T$  in the wrapper wall to sustain such a heat flux would be  $\approx 1660$  K. Even then an impinging jet of the 3000 K melt upon the inner wall of the wrapper would lead to the critical heat flux at the outside of the wrapper in the sodium cooled channel.

## 6. Summary and Conclusions

In both experiments the first pin failure developed rather locally and showed smooth pressure increases or low pressure peaks only. Two failure modes were observed: in case of moderate gas pressure in the pins there was boiling in some subchannels prior to pin failure, at higher gas pressure the pin failed into unvoided subchannels. In neither case a FCI by the injection of melt into the subchannels was registered nor an accumulation of molten material transported inside the pins into the vicinity of the local failures. The dominant flow regime in the pins seems to be of annular mist flow type.

The main gas volume from the pins was released very fast within 100-150 ms after first pin failure. The gas initiated a fast expulsion of liquid sodium from the bundle which took place prior to the melting of major parts of the pins. The time interval for voiding the testsection up to the ends of the dummy zones was found to be approximately inverse proportional to the original gas pressure in the pins. It can be concluded from the X-ray cine films that the small quantity of dispersed melt injected via the local leaks into the subchannels was carried away very fast by the expanding gas.  $\sim 60$  ( $V_{Th74}$ ) and  $\sim 130$  ms ( $V_{Th79}$ ) after the first pin failure major parts of the pins in the lower thermite zone were molten. Liquid sodium fed into the thermite zone from below led to low energetic FCIs and sodium flash evaporation generating the driving pressure for the main material dispersion and movement.

Within  $\sim 150$  ms of the first pin failure rather tight blockages have been built up in the upper dummy zone and some time later however less tight also in the lower dummy zone. At that time a major quantity of material is already removed from the thermite zone and relocated in the simulated breeding zones. So the main material movement seems to be dominated by the expanding sodium vapour generated by thermal reactions with molten material in the lower part of the thermite zone.

In both experiments the first bundle wrapper failed locally but at very different times. This caused a fast pressure relief but also a material transport away from the thermite zone via the annular channel surrounding the first wrapper. Blockages did not build up in the annular channel.

With respect to mild TOP or LOF/TOP transients the experimental results indicate qualitatively the following characteristics:

- An axial transport of fuel inside the pins towards local failures in the center of the core seems to be rather small. The fuel injected into the subchannels is removed very fast by expanding gas. So the reactivity increase by fuel motion towards the core center should be small or even negligible.
- Local FCI's and flash evaporation of sodium have a significant dispersal potential which will help to shut down the reactor transient.
- During the transient dense blockages can build up in the breeding zones, so enclosing the fuel region. However this should not occur prior to a major fuel removal from the core midplane region.
- Local failures of the subassembly wrappers initiate a pressure relief from the fuel region together with a remarkable removal of molten materials via the channels between subassemblies.

It should be kept in mind that a direct quantitative transfer of the described experimental results to reactor conditions is not feasible. The main object of the experiments is to provide data for validation of codes like CALIPSO.

7. Literature

- [1] P. Menzenhauer, W. Pepler, H. Will:  
Unveröffentlichter Bericht 1981
- [2] F. Kedziur:  
CALIPSO - Ein Programm zur Berechnung von Fluidodynamik,  
Thermodynamik und Geometrieänderungen in versagenden Brennelementen eines schnellen Brutreaktors.  
KfK-Bericht 3363/Juli 1982
- [3] P. Menzenhauer, S. Misu, W. Pepler, H. Will:  
Simulation of Mild TOP Accidents in Fast Breeder Reactors using  
Thermite filled Fuel Rod Simulators  
Intern. Symp. on Fuel Rod Simulators, Oct. 21-24, 1980,  
Gatlinburg, USA
- [4] P. Menzenhauer, St. Misu, H. Will:  
Unveröffentlichter Bericht 1981
- [5] P. Menzenhauer, St. Misu, H. Will:  
Unveröffentlichter Bericht 1981
- [6] H. Lurie, R.C. Noyes:  
Boiling Studies for Sodium Reactor Safety, Part II  
NAA-SR-9477

Annex: Matrix of the SIMBATH Tests

In the two tables X and XI the tests executed and planned up to the year 1986 are summarized. It should be kept in mind that these tables give a tentative survey only. The actual test program is undergoing a permanent change due to an increasing knowledge from new tests, consideration concerning code development and verification and of course results from other research work.

When the use of Uranium-Thermite ( $U-Fe_2O_3$ ) has been proven to be feasible more tests will be done with this thermite.



Measured variable	Transducer/error	Amplifier/ error	Total error in the measuring range	Signals concerned	
				Test $V_{Th}^{74}$	Test $V_{Th}^{79}$
Flow	permanent magnetic flow meter / 4 %	differential / $\pm 0.1 \%$	$\pm 0.3 \text{ m}^3/\text{h}$ )1 $\pm 0.1 \text{ m}^3/\text{h}$	D1T-D3T; D2K D4T	D1T-D3T; D2K D4T
Temperature	thermocouples / $\pm 0.75 \%$	differential / $\pm 0.1 \%$	$\pm 7.5 \text{ }^\circ\text{C}$ 2)2	CT1-CT11; T41 T42;	CT1-CT6; T7-T13
Dynamic pressure	piezoelectric transducer / $\pm 0.4 \%$	capacity and differential $\pm 1 \%$	$\pm 2 \text{ bar}$	P1-P6	P1-P5
Void	Chen type system 3 lead thermocouple	frequency carrier and differential	-	CT1-CT11	CT1-CT6
Current voltage	current and voltage transformer, the former with shunt / $\pm 0.5 \%$	differential $\pm 0.1 \%$	$\pm 0.7 \text{ A}$ $\pm 0.3 \text{ V}$	I1-I7 U1-U7	I1-I7 U1-U7
Static pressure	Barton cell / $< \pm 0.7 \%$	differential $\pm 0.1 \%$	$\pm 0.18 \text{ bar}$ )3	POB; P1B; P2B	POB; P1B; P2B

)1 Flow meters are calibrated prior to each test; so the relative error is much smaller than the absolute error as indicated

)2 It can be shown from isothermal measurements that the actual error is smaller than  $4^\circ\text{C}$ . The CT-thermocouples are always with 3 leads and grounded, o.d. 0.5 mm / T41; T42 of  $V_{Th}^{74}$  and T7; T8 of  $V_{Th}^{79}$  insulated type, o.d. 1.0 mm / T9 - T13 of  $V_{Th}^{79}$  insulated type, o.d. 0.5 mm

)3 Calibrated prior to test

Table I Overview of Measuring Chains

Test No		V <sub>Th</sub> 74	V <sub>Th</sub> 79
Initial temperature (before ignition)	K	767	767
Initial pressure within pin (before ignition)	bar	0	16
System pressure in the center of the test-section	bar	2.64	2.1
Pressure in the pin after reaction (~2500 K)	bar	50	100
Sodium velocity in the bundle, 1 m/s ~ 0.68 m <sup>3</sup> /h	m/s	4.16	4.6
Sodium velocity in the annular channel, 1 m/s ~ 2.4 m <sup>3</sup> /h	m/s	0.42	0.20

General data:

Length of upper simulated breeding zone	450 mm
Length of lower simulated breeding zone	800 mm
Hydraulic diameter	3.04 mm
Flow cross section of bundle	190 mm <sup>2</sup>

Table II Test Parameters of the 7-Pin Bundle Experiments

V<sub>Th</sub> 74 and V<sub>Th</sub> 79

t ms	Bundle						Remarks
	P1/t <sub>1</sub> bar/ms	P2/t <sub>2</sub> bar/ms	P3/t <sub>3</sub> bar/ms	P4/t <sub>4</sub> bar/ms	P5/t <sub>5</sub> bar/ms	P6/t <sub>6</sub> bar/ms	
-	1.9 <sup>x</sup>	1.71	1.24	0.89	0.12	0.04	Steady pressure due to friction at a flow in the bundle of 2.85 m <sup>3</sup> /h (~4.16 m/s) and in the annulus of 1.6 m <sup>3</sup> /h (~0.42 m/s) prior to the test
16							First detectable pressure disturbance (1)
51							Beginning of a series of pressure peaks indicating boiling and condensation
101	27/1	37/1	14/1	35/1	35/1	6.4/2	Maximum values during boiling which do not appear exactly at the same time
117	7	7	1.6	1.6	1.6	~0	Pressure peaks disappear, a steady pressure remains
134	194/0.5	100/0.5	~2	~2	~0	~0	Pressure peaks at P1 and P2 from pin failure, followed by a hump in the steady pressure (duration 22 ms) (2)
147	16	19	~2	~2	~0	~0	Maximum pressure of hump
156	4	4	46/0.7	~0	~0	~0	Pressure peak at P3
168	6	7	118/0.7	~2	~0	~0	Pressure peak at P3
232	6	5	121/0.5	3	~1.6	~1.6	Beginning of a series of pressure peaks at P3 and P4 (3)
250	25/1	35/1	17	35/0.7	~0	~0	Pressure peak at P4 and ~4 ms later also at P1, 2 and 3 followed by a pressure hump (duration 35 ms); bundle structure disintegrated (4)
265	21	21	21	18	30/1	~0	Maximum of hump at P5
396	29/1	37/1	122/1	37/1	78/0.7	~0	Begin. of a series of pressure peaks changing over into a pressure hump (duration ~30 ms)
411	20	24	26	24	22	~0	Maximum pressure of hump
522	42/0.7	52/1	24/1	16/1	~1	~0	see time 396
539	10	20	22	22	4	~0	see time 411 (6)
861	27/1	76/0.7	10/1	17/1	~0	~0	see time 396
875	12	30	29	22	~0	~0	see time 411, time 894 ms local failure of wrapper

Some further pressure events of minor importance are observed until time 1992 when the test is finished (7)

t<sub>1</sub> - t<sub>6</sub> refer to the approximated duration of the peak

○ Numbers of the important events in diagram No 4 (the time in this table may not be exactly the same as in the diagram)

x estimated

Table III Survey of Pressure Events V<sub>Th</sub> 74

t ms	Bundle				Annulus	Remarks
	P1/t <sub>1</sub> bar/ms	P2/t <sub>2</sub> bar/ms	P4/t <sub>4</sub> bar/ms	P5/t <sub>5</sub> bar/ms	P3/t <sub>3</sub> bar/ms	
-	1.36	0.9	0.6	0.2	0.044	Steady pressure due to friction at a flow in the bundle of 3.2 m <sup>3</sup> /h (~4.6 m/s) and in the annulus of 0.59 m <sup>3</sup> /h (~0.24 m/s) prior to the test
87	-	-	-	-	-	First detectable pressure disturbance
88	38/0.6	12/~1	27/0.8	12/0.8	~0	Pressure peaks followed by a hump in the steady pressure (duration ~22 ms) ①
101	12	12	10	8	6.3	Maximum pressure of hump
215	150/0.6	4	2.3	3.0	4	Pressure peak at P1 ③
218	-	53/0.8	2.3	3.0	4	Pressure peak at P2
229	11	14	2.3	3.0	2.3	Pressure hump at P1 and P2 (duration (duration ~20 ms)
426	31/0.8	4	2.0	2.0	8/~1.0	Pressure event at P1, 2 and 3 only
429	-	16/~1.0	-	-	-	Pressure peak at P2
544	98/0.6	2.0	1.5	1.5	18/1.0	Pressure peaks at P1 and P3 followed by a pressure hump (duration 20 ms) ⑤
553	6.0	9	1.5	1.5	9	Maximum of pressure hump
622	31/0.7	1	0	0	2	Pressure peak at P1
636	2	~5	0	0	~5	Steady pressure at P1, 2, 3 continues for some time ⑥
717	20/0.8	2.3	0	0	0	Pressure peak at P1
720	50/1.0	3.0	0	0	4	Pressure peak at P1, pressure increase at P2 and P3

No further pressure events of importance after ~ 750 ms

t<sub>1</sub> to t<sub>5</sub> refer to the approximated duration of the peak

Cover gas pressure ≈ 1.1 bar (absolute)

○ Numbers of the important events in diagram No 8 (the time in this table may not be exactly the same as in the diagram)

Table IV Survey of Pressure Events V<sub>Th</sub> 79

t ms	Lower X-ray viewing area	Center X-ray viewing area	Upper X-ray viewing area
Sequence of ignition: No of pin/time 5/0; 1/62; 2/77; 3/77; 4/82; 6/82; 6/88; 7/103			
117	First pin failure, Material moves upw. -12ms	no event visible	no event visible
145	Material moves downwards		
156	Pins disintegrate along the lower half		
178	All pins are disintegrated		
	Material from the lower 2/3 moves downwards		
221	Pressure front from below leads to the dispersion of material		
231	Material moves upwards v = 4.30 m/s		
	Material density decreases		
243	Dispersed material of different density moves upwards		
250	Compaction pressure front from above (3)		
258	Material moves upwards v = 5.8 m/s (4)		
264	Material of low density moves upwards, high density at the wall (annular flow!)		
274	Wrapper nearly empty		
284	Compacted material starts to move downwards v = 3.6 m/s (5)		
314			
385			
396	Material of different compaction moves downwards		
404	Pressure front from below, material is dispersed		
411	Finely dispersed material moves upwards	Material moves upwards v = 6.2 m/s	Material compacted to high density Material compacted to high density Compacted material melts out of the lower third of this area Compacted material moves downwards from the lower third Compacted material
454	Material with particles moves slowly upwards		
486	Material with particles moves slowly upwards		
530	Pressure front from below leading to material dispersion		
533	Upward acceleration of material		
539	Finely dispersed material moves upwards (6)		
639			
761	Compacted material moves downwards along the viewing area within 86 ms v = 2 m/s		
767			
861	Material has a high density (6)		
867	Pressure front from below leading to material dispersion within 1 ms	Compacted material moves downwards	High density material
869	Material moves upwards v = 10.5 m/s		
871			
873			
875	High material velocity upwards, material density in viewing area decreasing		
887			
895			
935			
947	Material moves upwards v = 2 m/s		
979			
1038	Wrapper nearly empty, pressure front leads to dispersion within 6 ms	Pressure front from below leading to dispersion	Material arrives from below v = 10 m/s
1086			
1130	Compacted material moves downwards along the viewing area within 87 ms		
1241			
1249	Individual material agglomerations falling through viewing area		
1256	Pressure front from below leading to dispersion, material moves upwards		
1261			
1262	Material eddy in viewing area without definite axial velocity		
1268	Material moves upwards slowly		
1285	Material moves downwards slowly		
1297		All material moves downwards	Lower third of wrapper is loaded with material of high density
1622			
1685	Material moves downwards slowly		
1757			
1990	Molten material still visible in the lower part (7)		
1996	Pressure front from below, material moves upwards		
2014			
2016	Pressure front from above, material moves downwards		
2063	Flow reversal		
2190	Material falls into viewing area from above		
2150	Material concentration in the lowest part of the viewing area, material movement finished	Leakage of test-section into surrounding, X-ray viewing area masked within 113 ms	Upward material movement in annulus Compacted material moves downwards
		further events obscured	Material movement in the annulus finished Material concentration in the lower third is low
		Material movement finished	Small pressure front material moves downw.

v refers to an estimated material velocity (molten material) No (2), (5), (7) to the events in diagram No 4 (the time in this table may not be exactly the same as in the diagram)

Table V Test V<sub>Th</sub> 74 Observations from the X-Ray Cine Films

t ms	Lower X-ray viewing area	Center X-ray viewing area	Upper X-ray viewing area		
Sequence of pin ignition: No of pin/time 4/0; 2/7; 3/89; 6/127; 7/140; 1/143; 5/151; at t = 93 ms first flow reversal					
88	First pin failure in level 130 mm	no event visible			
109	Pin structure masked (first visible event)				
116	Material moves upwards, pin structure still visible in the upper part				
190	All pins have failed?				
214	Material moves upwards $V_m = 1$ m/s (3)				
223	Pressure front from below leads to the dispersion of material $v = 42$ m/s				
228	Dispersed material moves upwards $v = 5$ m/s				
233	Material moves downwards from the upper edge of the viewing area $v = 5$ m/s				
244				Bundle structure masked from below	no event visible
				Material concentration	
250	Material arrives at the lower edge $v = 5$ m/s				
265	Material moves downwards $v = 4$ m/s				
284	Material density decreases				
297	Material moves upwards in the annular channel (4)				
311	Compaction of material from above				
350	Material moves upwards in the annular channel				
378		Material moves upwards in the annular channel $v = 5$ m/s			
394		Material moves upwards in the annular channel; lower third of pins disintegrated			
425	Pressure front from below $v = 17$ m/s; material moves upwards	no event visible			
435	Melt through of wrapper in the lower third of this part				
441	Material moves upwards $v = 8$ m/s				
480			Material from the lower third moves downwards. Material compaction in the center		
486	Material reversal; compaction of material from above at the upper edge				
525	Material moves downwards $v = 6$ m/s (5)		Material from the center moves downwards, pins in the thermite region disintegrated		
543	Material inside the wrapper moves downwards Material inside the annular channel moves upwards				
555			Pressure front with material compaction from below, 3 ms later material moves downwards again		
566	Low material concentration in the lower third				
592	Material moves downwards $v = 5$ m/s		Material moves downwards $v = 7$ m/s, low material concentration in the lower half Material compaction in the upper third, material decreases in the lower half		
631	Pressure front from below, flow reversal	no event visible			
635	Material moves upwards $v = 9$ m/s				
641	(6)		Pressure front from below, material compaction		
648			Material compaction in the upper half, flow reversal		
681	Flow reversal		Material moves downwards $v = 8$ m/s		
716	Material moves downwards		Lower half nearly emptied of material		
726	Flow reversal, material moves upwards				
769	Large melt through towards the annular channel				
779	Material of low concentration moves downwards				
948			Compacted material moves downwards from the center of the viewing area		
1058		Material leaves viewing area downwards $v = 1$ m/s			
1222	Compacted material appears at the upper edge of the viewing area $v = 1$ m/s (7)	no event visible			
1282	Pressure front from below leads to dispersion of the compacted material				
1468			Lower 2/3 of the wrapper section nearly emptied of material		

v refers to an estimated material velocity (molten material) No (3) to (7) to the events in diagram No. 8  
(The time in this table may not be exactly the same as in the diagram)

Table VI Test  $V_{Th}$  79 Observations from the X-Ray Cine Films

Pin cladding	[ mm ]	7.6 x 0.3	
Burst pressure of SS316 at 20/1000/1200 °C	[ MPa ]	750/140/25	
Temp. difference in the clad wall during boiling with 2000 W/cm <sup>2</sup> heat flux	[ K ]	~ 230	
Rate of temperature increase of the uncooled clad wall (film boiling ~15 ms)	[ K/ms ]	14	
Calculated cases		V <sub>Th</sub> 74	V <sub>Th</sub> 79
Pressure in the pin at 760 K prior to the test	[ bar ]	0	16
Pressure in the pin during reaction a gas release of 0.7 Ncm <sup>3</sup> per gramm of thermite and a gas temperature of 2500°K is assumed	[ bar ]	~50	~100
Calculated minimum wall thickness at different average wall temperatures	135 °C	0.025	0.05
	1115 °C	0.2	0.4
	1315 °C	1.52	3.04

Table VII Considerations concerning the Pin Failure Mechanism

t ms	Bundle							V <sub>G</sub> /V <sub>Tot</sub> %	Attention: Steady pressure due to friction added, see table...
	P1 bar	P2 bar	P3 bar	P4 bar	P5 bar	Total Void cm <sup>3</sup>			
117	8.9	8.9	2.8	2.5	1.7	25	0	Boiling prior to pin failure	
133	8.9	8.9	3.2	2.5	-	42	40	30 % of gas released from the pins ②	
147	17.8	20.7	3.2	2.9	1.7	68	~55	All pins have failed in the lower thermite section, 40 % of gas is assumed to be released	
232	7.8	6.7	4.2	3.9	1.7	240	92	All pins are disintegrated along the lower half of the thermite section, 70% of gas is released	
265	22.8	22.7	22.2	18.9	1.7	272	40	All pins are disintegrated in the thermite zone, 100% of gas is released, leakage through the bundle wrapper into the annulus	
411	21.8	25.7	27.2	24.9	22.1	360	34	Between t= 265 and 411 a blockage builds up in the upper and lower dummy zone, therefore the void grows primarily in the annulus	

Table: VIII Estimated Fraction of Gas in the Measured Void volume V<sub>Th</sub> 74

- 40 -

t ms	Bundle				Annulus	Total Void cm <sup>3</sup>	V <sub>G</sub> /V <sub>Tot</sub> %	
	P1 bar	P2 bar	P4 bar	P5 bar	P3 bar			
101	13.4	12.9	10.6	8.2	6.3	21	~ 63	First pin has failed at ML 130 mm, 30% of gas is assumed to be released from this pin
201	5.4	4.9	3.3	2.9	4.0	406	~100	All pins have failed in the lower thermite section, 45% of gas is released, leakage through the bundle wrapper into the annulus
228	12.4	14.9	2.9	3.2	2.3	479	79	All pins are disintegrated in the lower half of the thermite section, 70% of gas is released
425	4.4	4.9	2.6	2.2	4.0	1056	59	Pins in the thermite section are disintegrated, 100% of gas is released

Table: IX Estimated Fraction of Gas in the Measured Void Volume V<sub>Th</sub> 79


















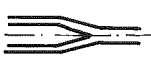





Number of Test	Main Aim	Experimental Set Up	Type of Thermite	Cross Section
14	Pin failure behaviour, material movement in the pin towards failure location	Single pin in stagnant sodium	Al-Fe <sub>2</sub> O <sub>3</sub>	
1	Material movement in the pins and the subchannels, material relocation	3-pins in stagnant sodium	Al-Fe <sub>2</sub> O <sub>3</sub>	
1	Material movement and relocation with fission gas simulation	7-pins in stagnant sodium	Al-Fe <sub>2</sub> O <sub>3</sub>	
6	Local pin failure behaviour	Single pin in stagnant water	Al-Fe <sub>2</sub> O <sub>3</sub>	
14	Pin failure behaviour, material movement in the pin and annular channel, influence of simulated fission gas pressure	Single pin in flowing sodium	Al-Fe <sub>2</sub> O <sub>3</sub>	
2 Subject of this report	Material movement and relocation, blockage build up, melt through of primary bundle wrapper and material movement in the annulus	7-pins in flowing sodium TOP characteristic	Al-Fe <sub>2</sub> O <sub>3</sub>	 Annulus with flowing sodium
1	As above	7-pins in flowing sodium LOF-characteristic	Al-Fe <sub>2</sub> O <sub>3</sub>	 As above
2	Stability of frozen crusts on convex-concave surfaces	Single pin in flowing sodium	Al-Fe <sub>2</sub> O <sub>3</sub>	
2	Measurement of temperature history of the cladding as an indicator of heat transfer processes	Single thick-walled pin in flowing sodium	Al-Fe <sub>2</sub> O <sub>3</sub>	

Table X SIMBATH, Matrix of Performed Tests

Number of Tests	Main Aim and Test Parameters	Experimental Set Up	Type of Thermite	Cross Section
2 83/84 <sup>1)</sup>	Feasibility of thermite with coated uranium particles	Single pin in stagnant sodium	U-Fe <sub>2</sub> O <sub>3</sub>	
3 84/85	Pin failure behaviour, material movement in the pin and annular channel, influence of simulated fission gas pressure, comparison with Al <sub>2</sub> O <sub>3</sub> thermite results	Single pin in stagnant sodium	U-Fe <sub>2</sub> O <sub>3</sub>	
1 84	Pin failure behaviour, transient heat transfer	Single pin in flowing sodium	Al-Fe <sub>2</sub> O <sub>3</sub>	
2 83...85	Behaviour of pins with increased diameter	Single pin in flowing sodium	Al-Fe <sub>2</sub> O <sub>3</sub>	 Outer wall of annulus Al <sub>2</sub> O <sub>3</sub>
2 83...85	Material movement and blockage build up with pins of cosine axial power distribution	Single pin in flowing sodium	Al-Fe <sub>2</sub> O <sub>3</sub>	
2 83/84	History of pressure and material release from a thick-walled pin with prefixed failure location, flow regime	Single pin in an empty channel	Al-Fe <sub>2</sub> O <sub>3</sub>	 Thick-walled cladding
3 83/84	Simulation of TRAN series II with Al-Fe <sub>2</sub> O <sub>3</sub> thermite, comparison with UO <sub>2</sub> behaviour	Thermite injector with attached annular channel	Al-Fe <sub>2</sub> O <sub>3</sub>	 TRAN-II
2 84/85	Local pin failure behaviour	Short single pin in air	Al-Fe <sub>2</sub> O <sub>3</sub>	
2 85/86	Material movement and relocation, blockage build up, melt through of primary wrapper and material movement in the annulus	7-pins in flowing sodium, eventually cosine shaped power distr. LOF character.	Al-Fe <sub>2</sub> O <sub>3</sub> eventually U-Fe <sub>2</sub> O <sub>3</sub>	 Annulus with flowing sodium
2 83/84	As above	19-pins in flowing sodium TOP/LOF characteristic	Al-Fe <sub>2</sub> O <sub>3</sub>	 As above
2 85/86	" "	37-pins in flowing sodium TOP/LOF characteristic	Al-Fe <sub>2</sub> O <sub>3</sub>	 As above
2 86	" "	127-pins in flowing sodium LOF characteristic	Al-Fe <sub>2</sub> O <sub>3</sub>	 As above

1) Scheduled for year...

Table XI SIMBATH, Test Matrix up to Year 86

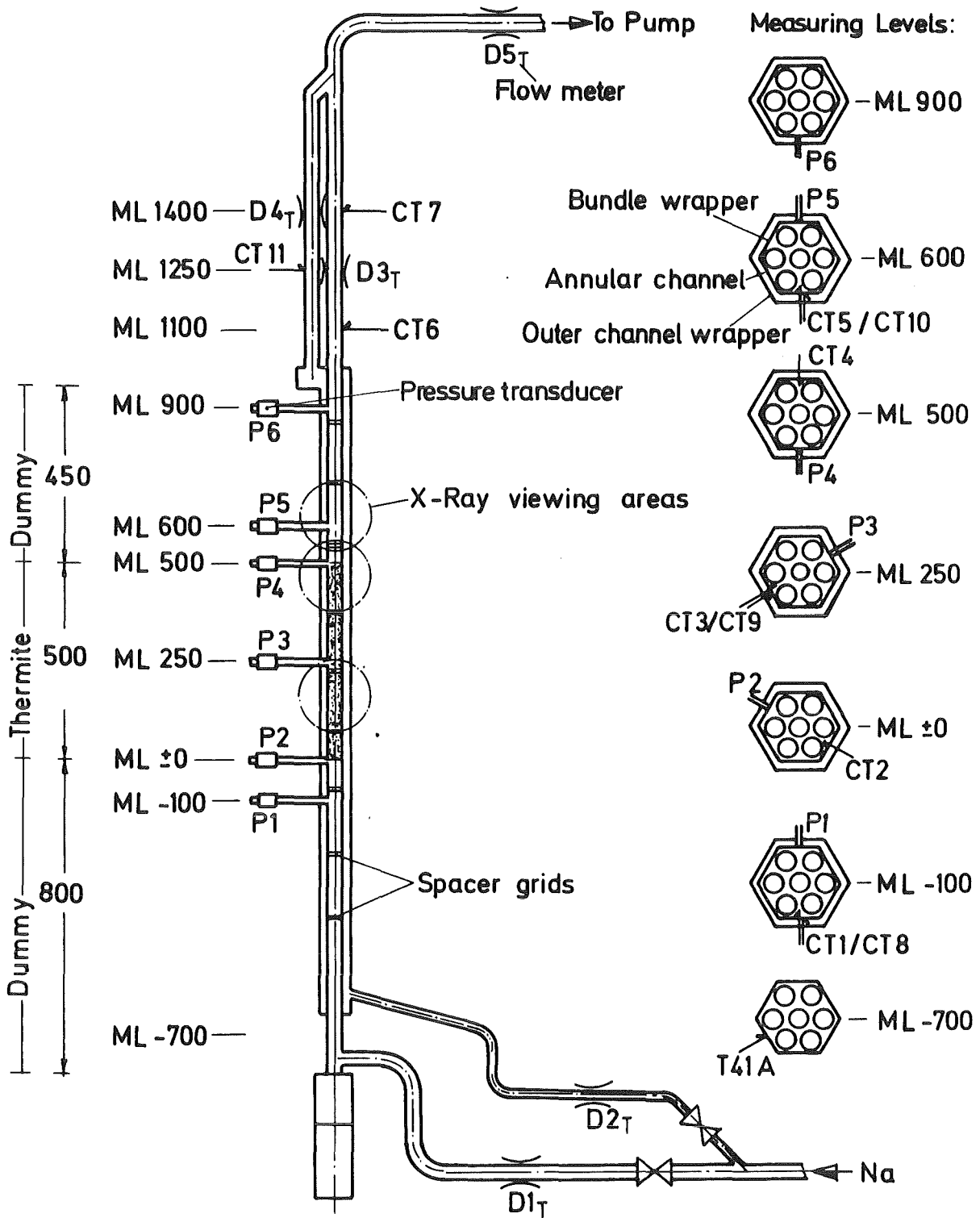


Fig. 1 Schematic Arrangement of 7 Pin Bundle for Test  $V_{Th} 74$

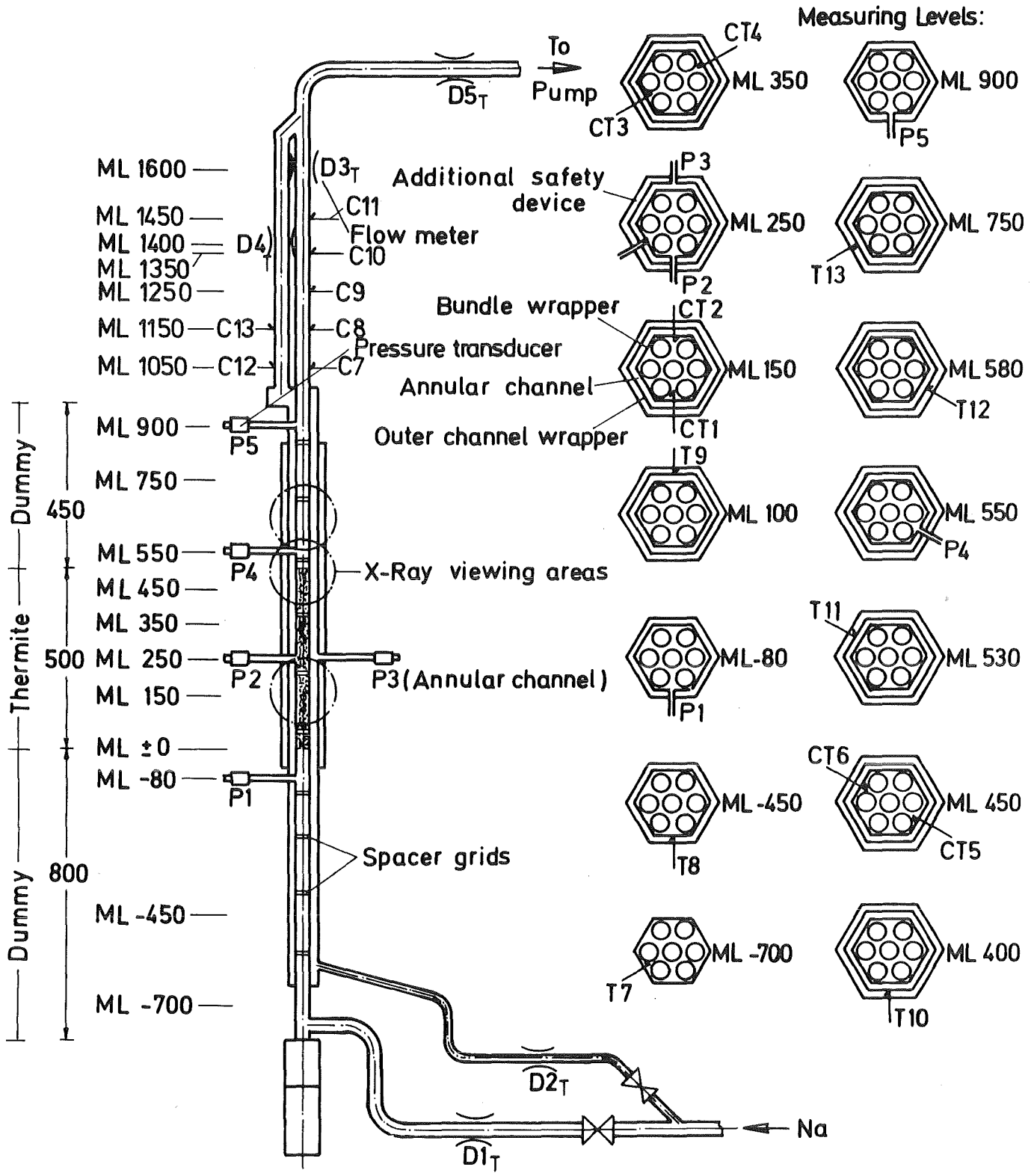
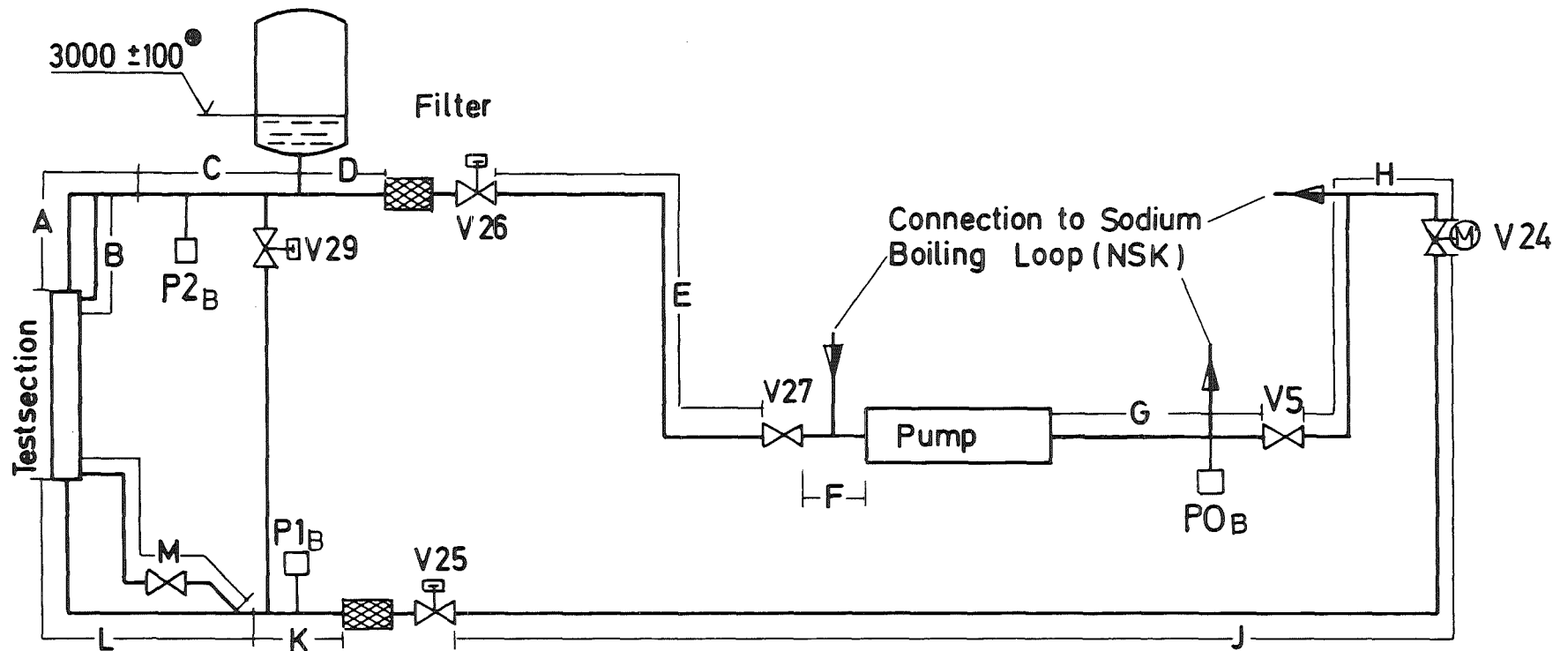


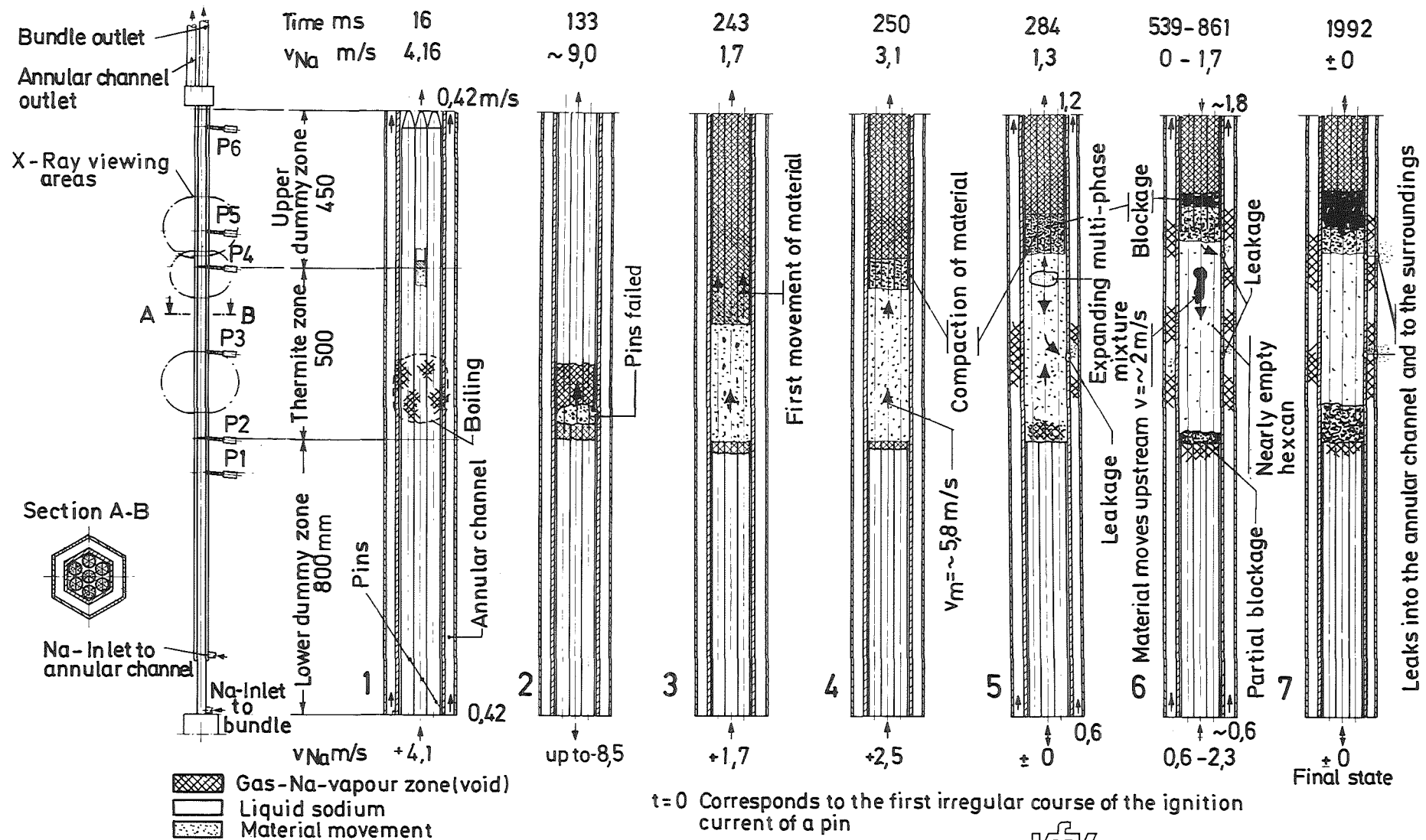
Fig. 2 Schematic Arrangement of 7 Pin Bundle for Test V<sub>Th</sub> 79



● related to the lower end of the thermite zone  $ML \pm 0\text{mm}$

Section	Inner diameter	Length (mm)	Bend 90°	Bend 45°
A				
B				
C	64,0	2500	3	
D	28,5	400		
E	28,5	7100	2	1
F	28,5	1400	2	
G	28,5	1100		1
H	28,5	2900	3	
J	28,5	8200	5	
K	28,5	1100		
L	20,0	1700	2	
M	12,0	1600	2	1

Fig. 3 Schematic Arrangement of the SIMBATH Loop



KIK IRE825369

Fig. 4 Important Events During Test  $V_{Th}$  74

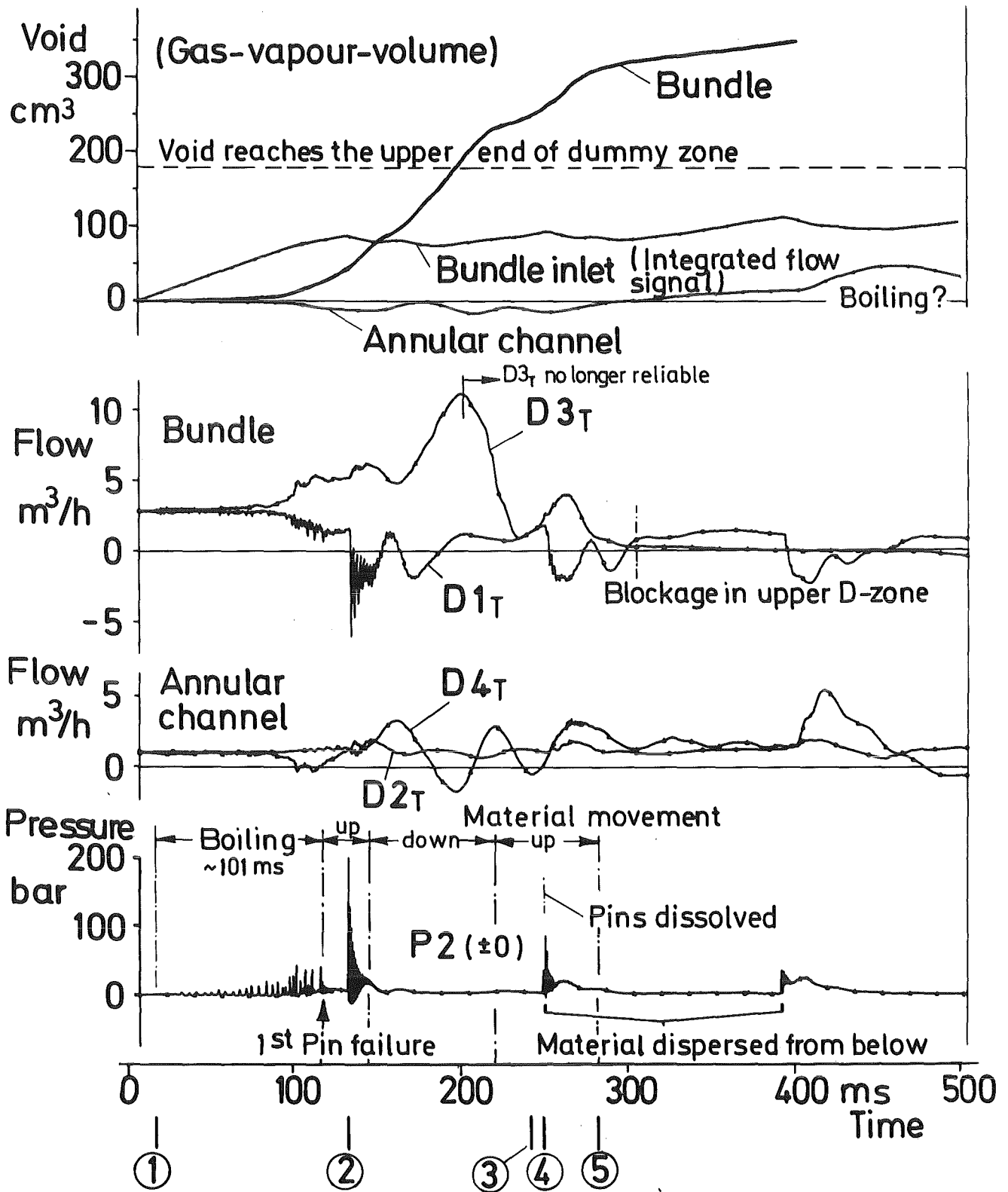


Fig. 5 Gas-Sodium-Vapour Volume, Flow, Characteristic Pressure (P2) V<sub>Th</sub>74

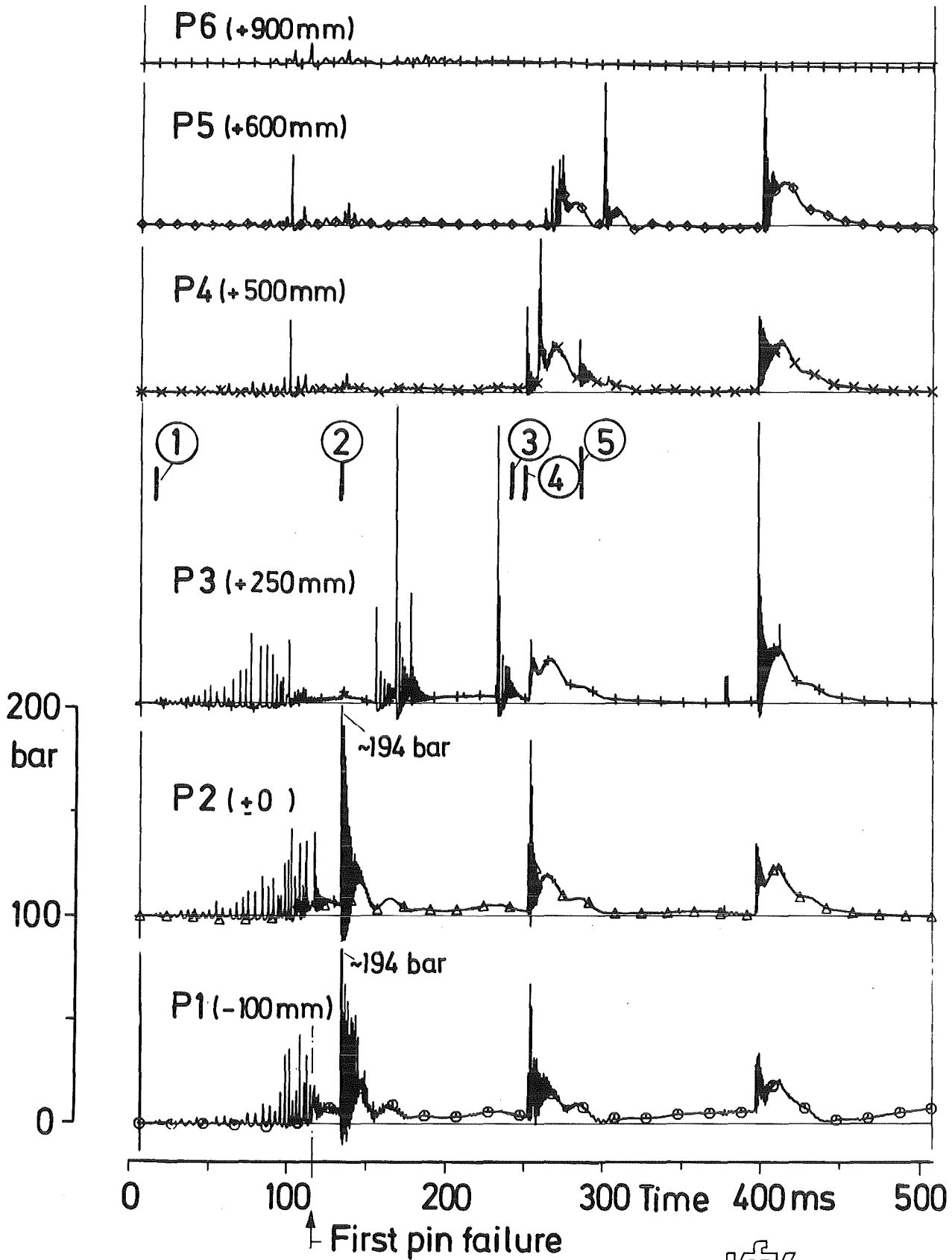


Fig. 6 Dynamic Pressure Behaviour of Test V<sub>Th</sub>74



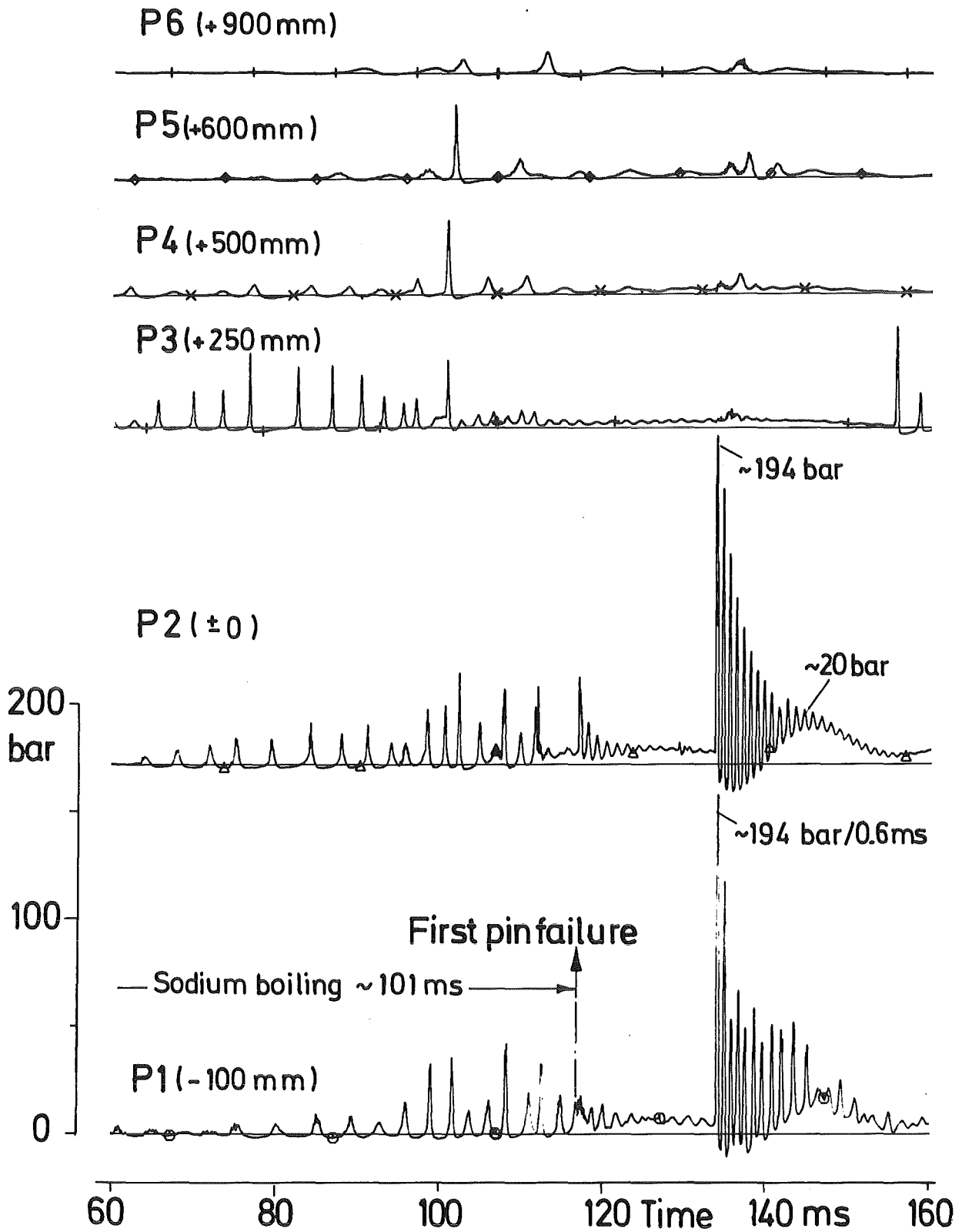
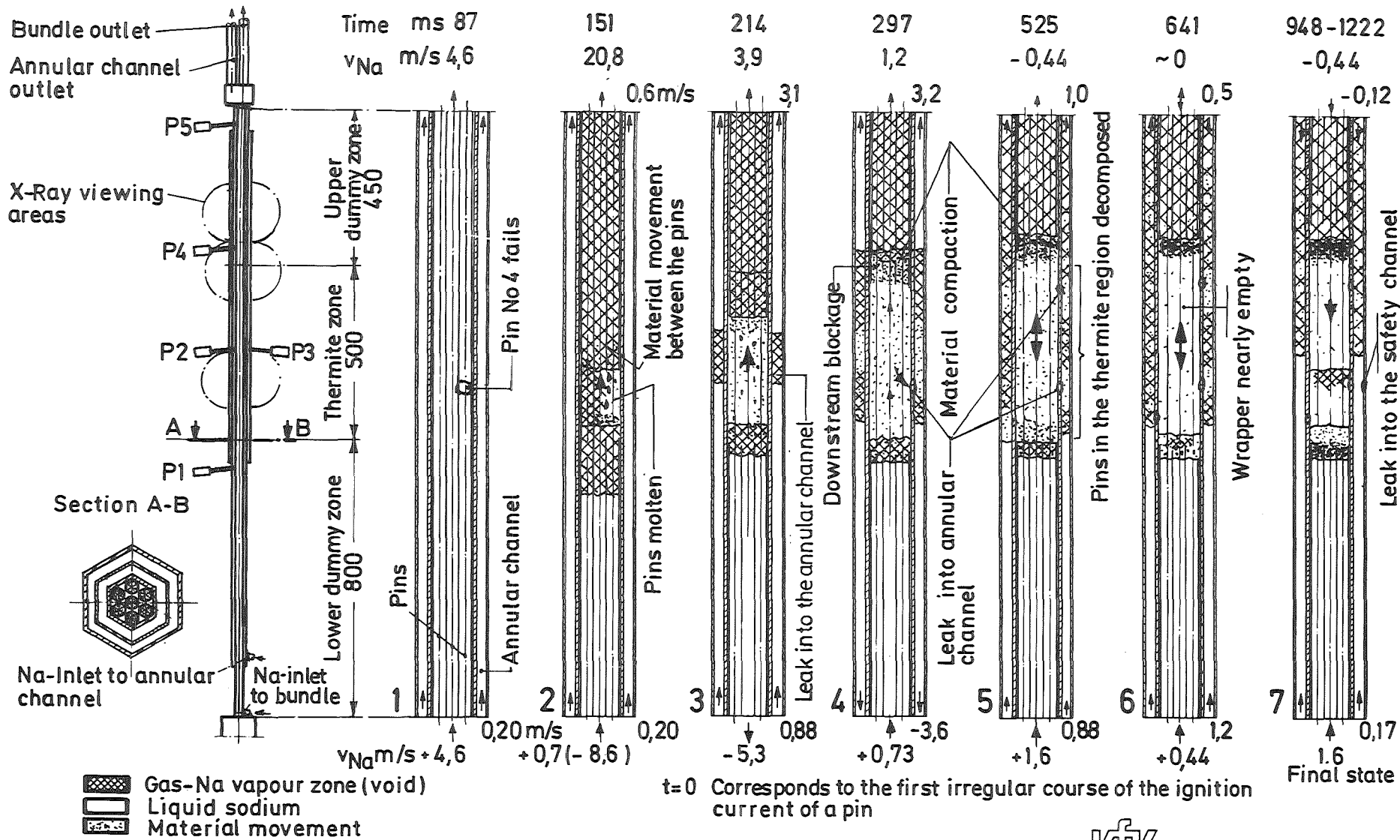


Fig. 7 Details of the Dynamic Pressure Behaviour for Test  $V_{Th}74$



KIK IRE825370

Fig. 8 Important Events During Test  $V_{Th}79$

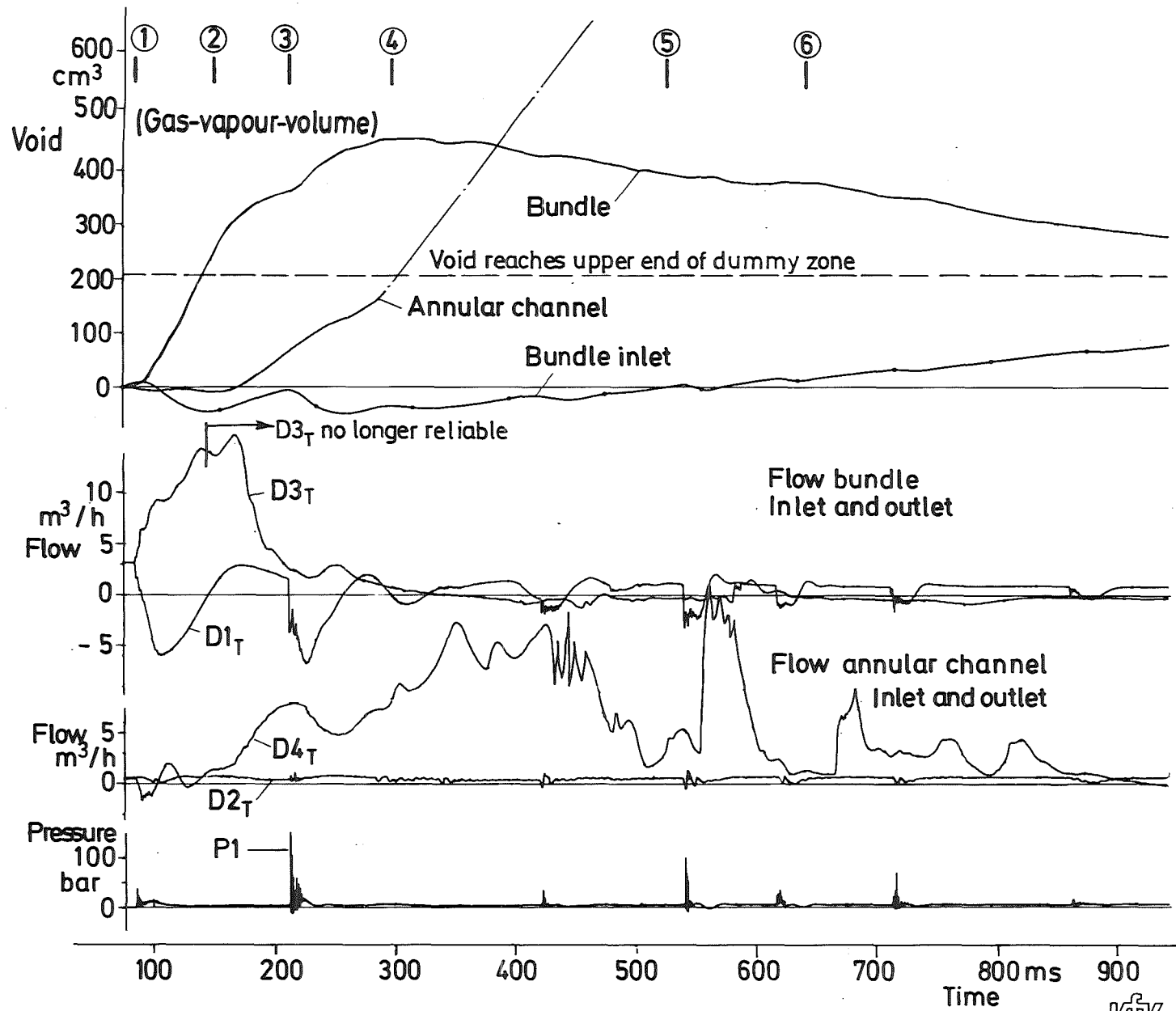


Fig. 9 Gas-Sodium-Vapour Volume, Flow, Characteristic Pressure (P1) V<sub>Th</sub> 79

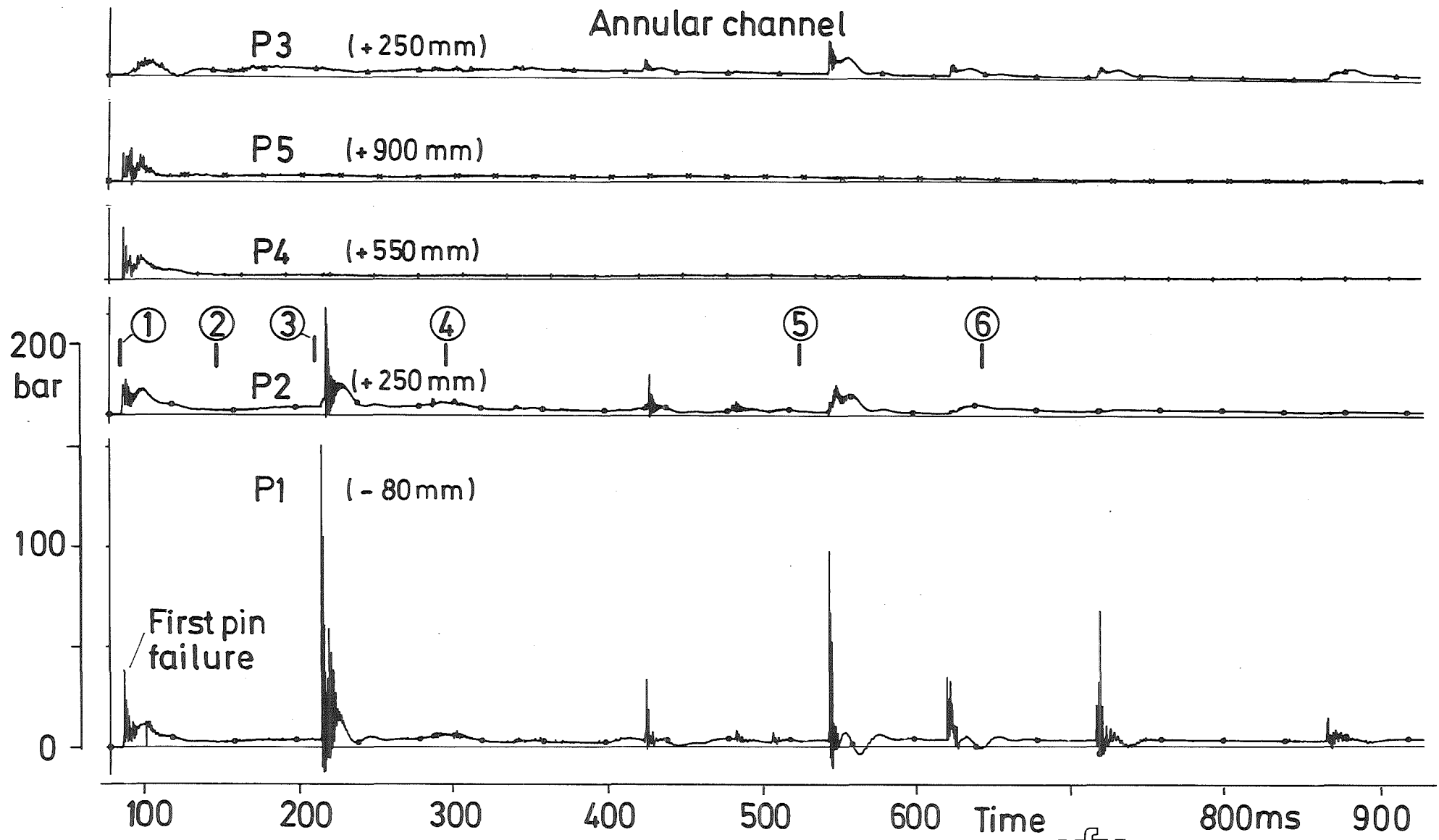


Fig.10 Dynamic Pressure Behaviour of Test  $V_{Th}79$

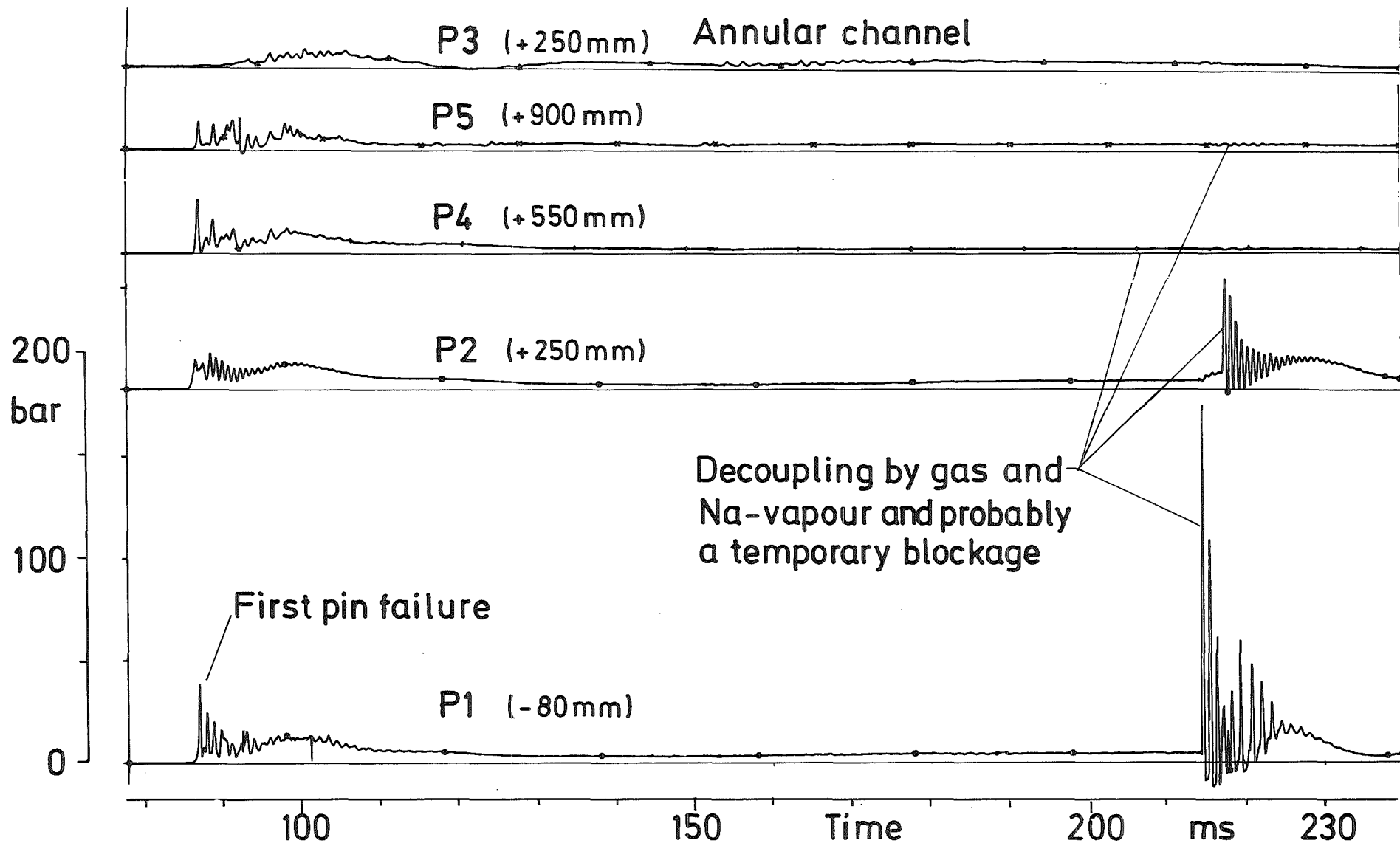


Fig.11 Details of the Dynamic Pressure Behaviour for Test V<sub>Th</sub> 79

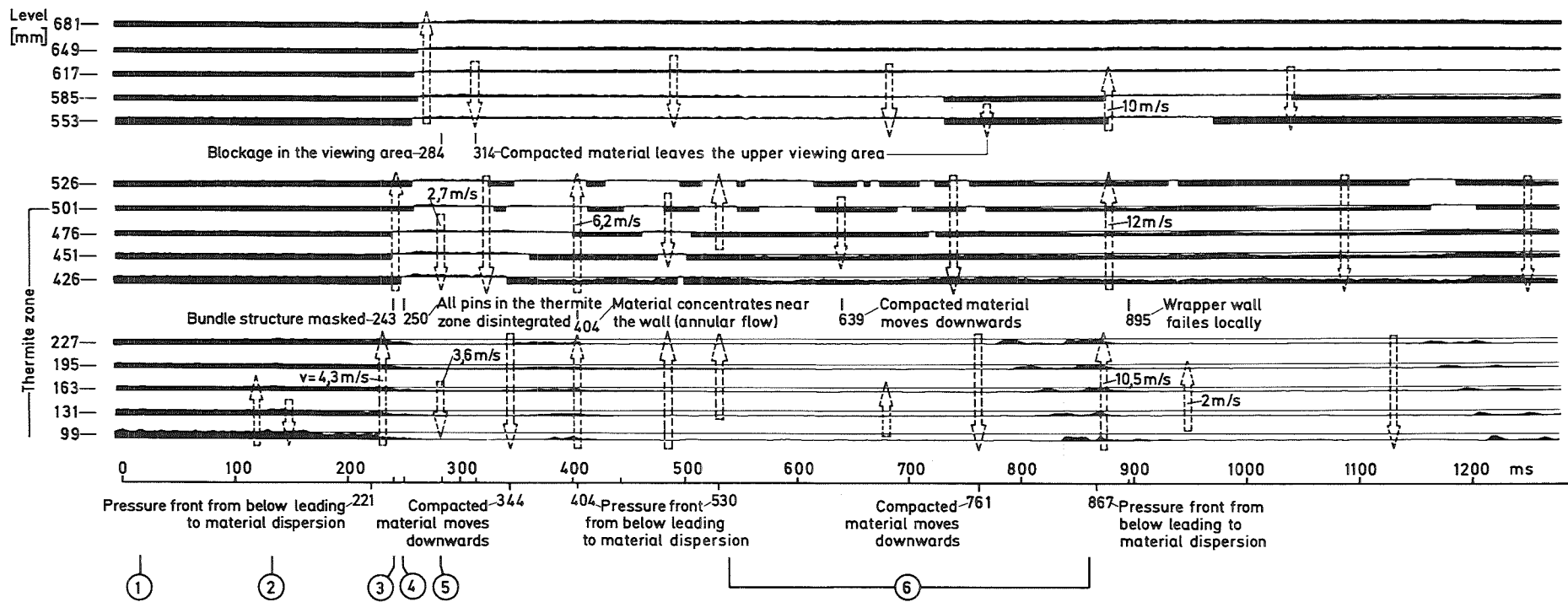


Fig.12 Redistribution of Material and Blockage Build Up  $V_{Th}$  74

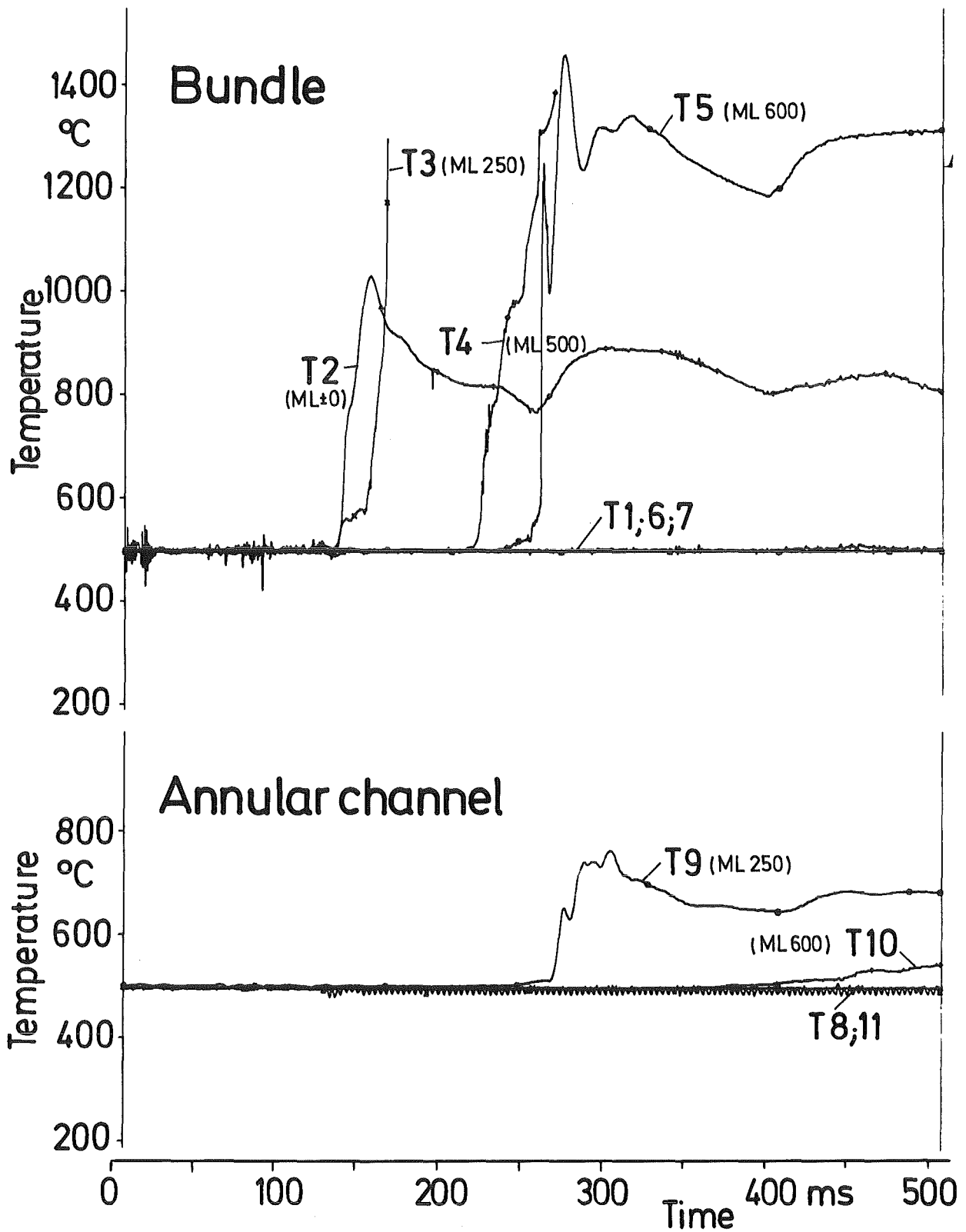
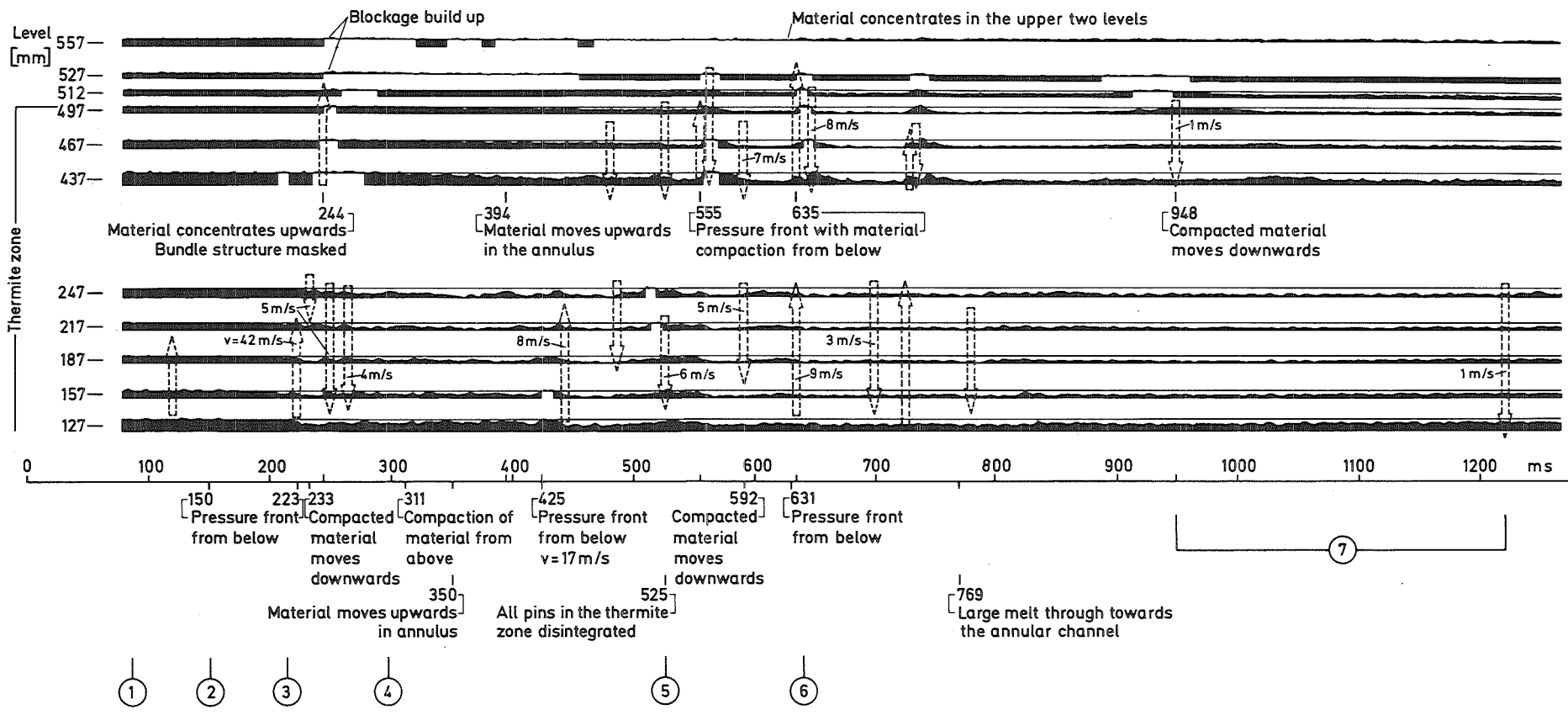


Fig.13 Course of Temperatures  $V_{Th} 74$



1  
56  
1

Fig.14 Redistribution of Material and Blockage Build Up  $V_{Th} 79$



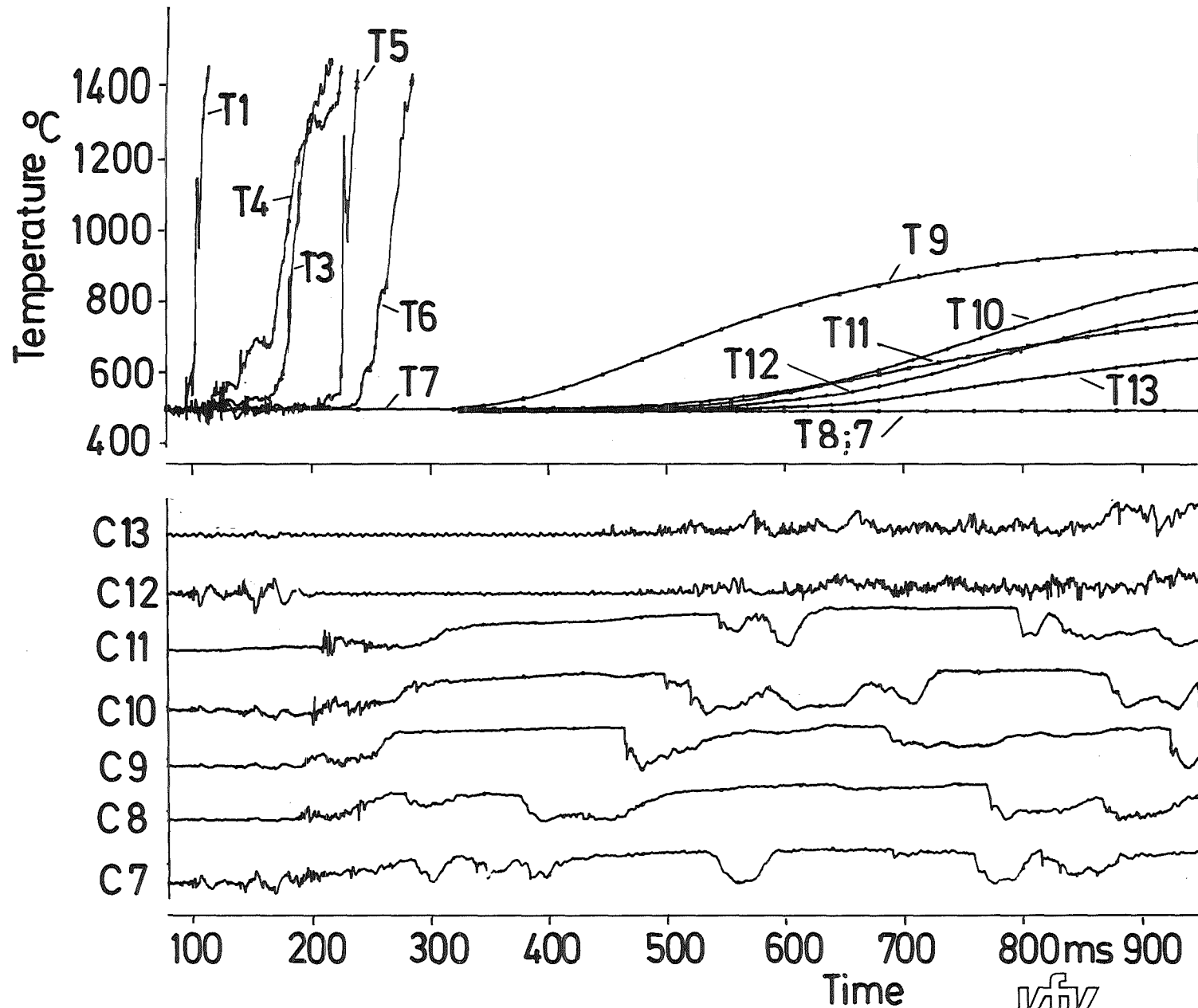
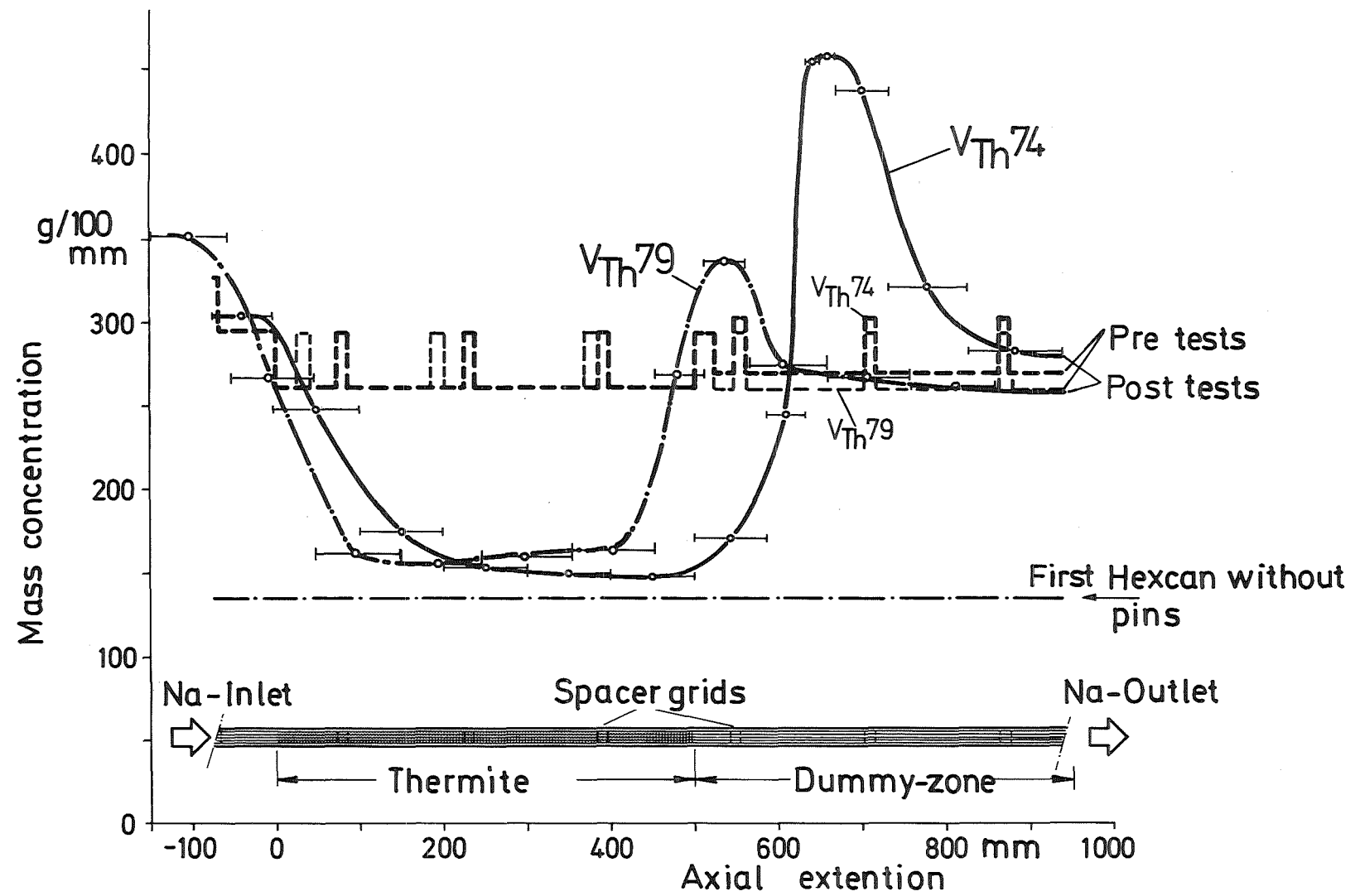
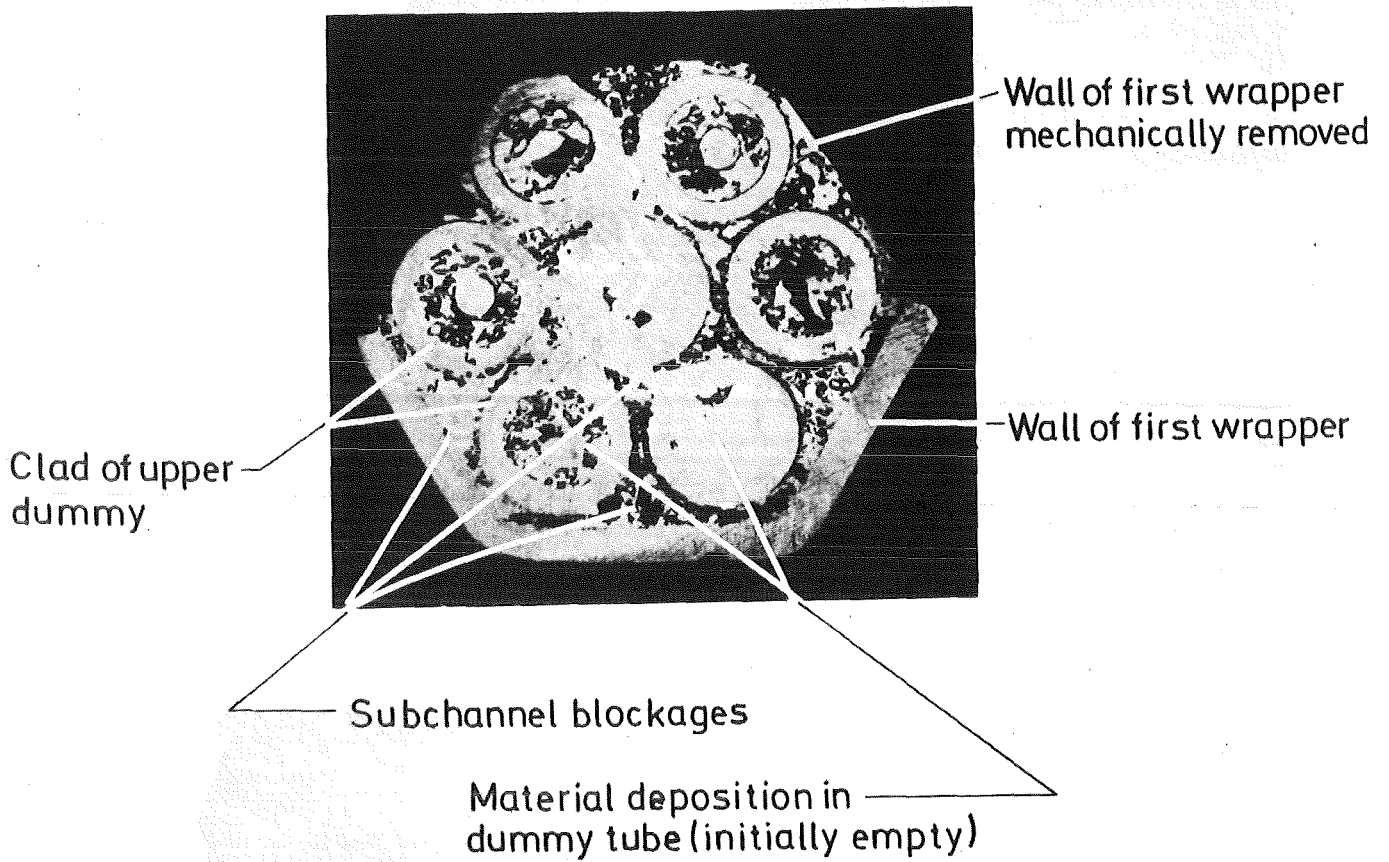


Fig.15 Course of Temperatures and Void Signals  $V_{Th79}$

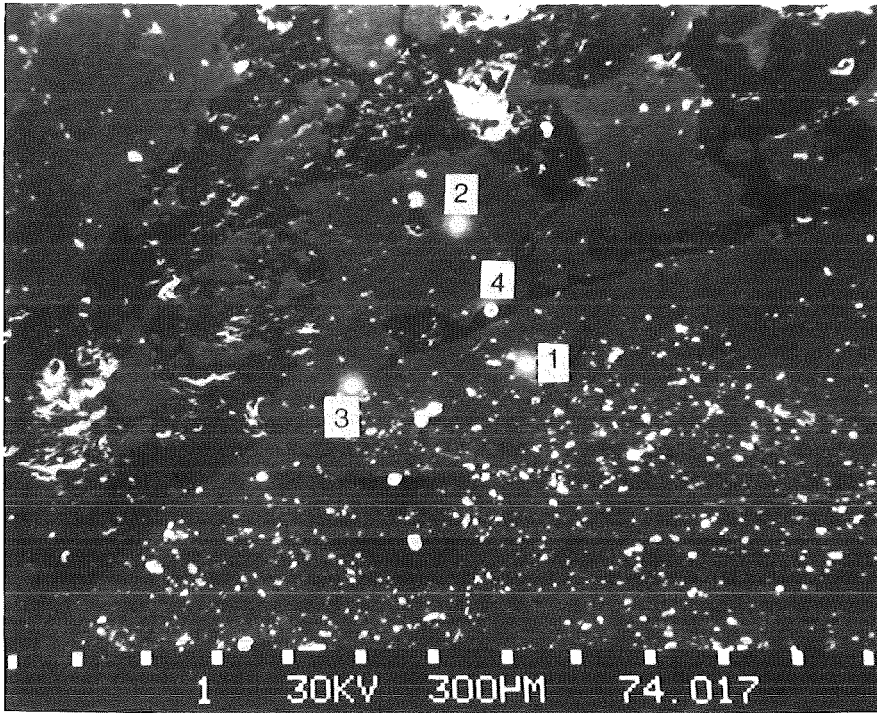


1  
8  
1

**Fig.16 Post Test Material Distribution in the Testsections  
V<sub>Th74</sub> and V<sub>Th79</sub>**



**Fig. 17 Cross Section of the Upper Blockage ( $V_{Th}74$ ; ML 667)**



- 1 Clad
- 2 Subchannel blockage
- 3 Clad blockage interface region
- 4 Blockage ( $Al_2O_3$  enclosure)

Fig.18 Enlarged Cross Section of the Upper Blockage with Spots for Local Analysis ( $V_{Th}$  74; ML 667)

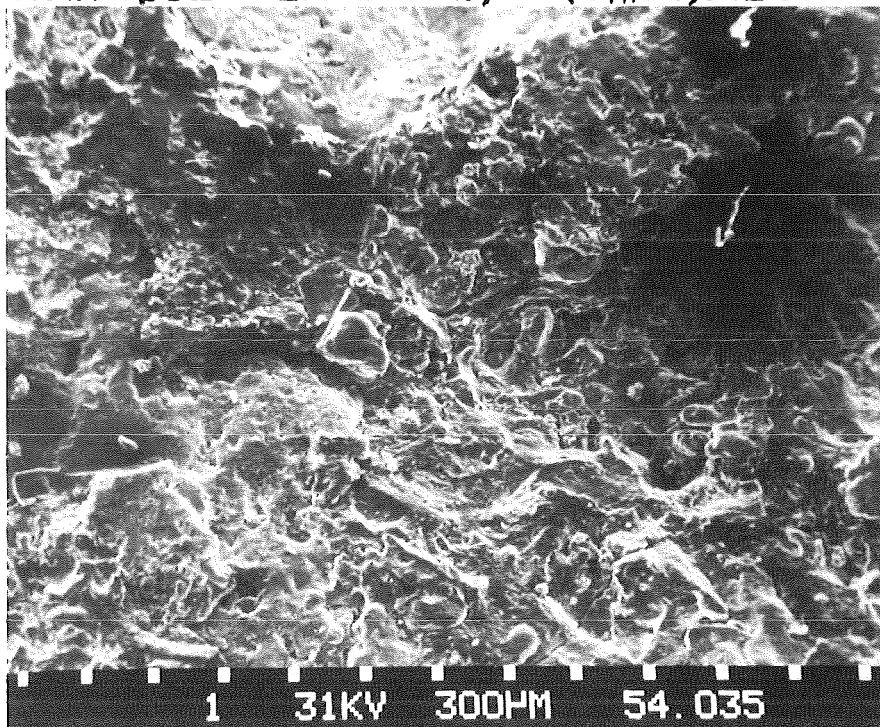


Fig.19 Surface Section of a Layer between the Blockage and the Wrapper Wall ( $V_{Th}$  74; ML 687)

KIK IRE833454

Fig.18 and 19 Post Test Analysis  $V_{Th}$  74

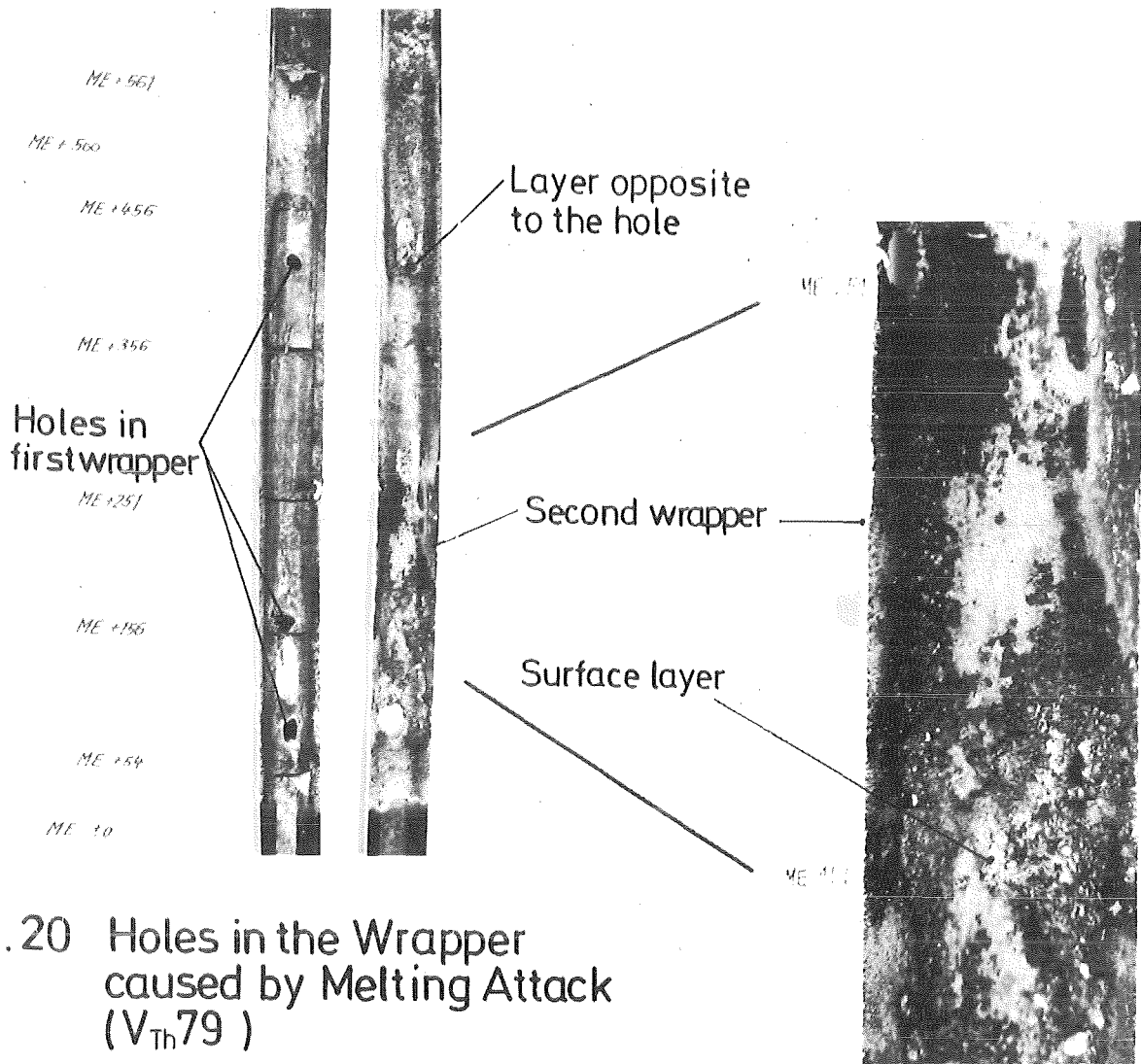


Fig. 20 Holes in the Wrapper caused by Melting Attack (V<sub>Th</sub>79 )

Fig. 21 Layer at the Inner Surface of the Second Wrapper ( V<sub>Th</sub>79 )

Fig. 20 and 21 First and Second Wrapper of Test Section V<sub>Th</sub>79